

1 **Hydroclimate variability in Scandinavia over the last millennium - insights from a**
2 **climate model-proxy data comparison**

3 Kristina Seftigen^{1,2,*}, Hugues Goosse², Francois Klein², Deliang Chen¹

4 ¹Regional Climate Group, Department of Earth Sciences, University of Gothenburg, Gothenburg, Sweden.

5 ²Georges Lemaître Centre for Earth and Climate Research (TECLIM), Earth and Life Institute, Université
6 catholique de Louvain (UCL), Belgium.

7 *Corresponding author:

8 E-mail address: kristina.seftigen@gvc.gu.se

9 **Abstract**

10 The integration of climate proxy information with General Circulation Model (GCM) results
11 offers considerable potential for deriving greater understanding of the mechanisms underlying
12 climate variability, as well as unique opportunities for out-of-sample evaluations of model
13 performance. In this study, we combine insights from a new tree-ring hydroclimate
14 reconstruction from Scandinavia with projections from a suite of forced transient simulations
15 of the last millennium and historical intervals from the CMIP5 and PMIP3 archives. Model
16 simulations and proxy reconstruction data are found to broadly agree on the modes of
17 atmospheric variability that produces droughts/pluvials in the region. Despite these dynamical
18 similarities, large differences between simulated and reconstructed hydroclimate time series
19 remain. We find that the GCMs simulated multidecadal/longer hydroclimate variability is
20 systematically smaller than the proxy based estimates, whereas the dominance of GCM
21 simulated high-frequency components of variability is not reflected in the proxy record.
22 Furthermore, the paleoclimate evidence indicates in-phase coherencies between regional
23 hydroclimate and temperature on decadal time-scales, i.e. sustained wet periods have often
24 been concurrent with warm periods and vice versa. The CMIP5/PMIP3 archive suggests, on
25 the other hand, out-of-phase coherencies between the two variables in the last millennium.
26 The lack of adequate understanding of mechanisms linking temperature and moisture supply
27 on longer time scales has serious implications for attribution and prediction of regional
28 hydroclimate changes. Our findings stresses the need for further paleoclimate-data model
29 intercomparison efforts to expand our understanding of the dynamics of hydroclimate
30 variability and change, to enhance our ability to evaluate climate models, and to provide a
31 more comprehensive view of future drought and pluvial risks.

32 **1. Introduction**

33 Among the current key priorities in climate research is a more comprehensive understanding
34 of changes in regional- to continental-scale hydroclimate in response to rising levels of
35 atmospheric greenhouse gases on time scales ranging from decades to centuries (Wu et al.,
36 2013; Hegerl et al., 2015). Delineating the role of internal variability and natural forcing, and
37 its contribution to the anthropogenically forced twentieth century climate (Zhang et al., 2007;
38 Sarojini et al., 2016), is immensely important for attributing past and predicting future
39 trajectories in the hydrological cycle, and for strategic approaches to adaptation and planning.
40 Sparse observational evidences limits possibilities of providing tight constraints on the long-
41 term behavior of the climate system. The longest instrumental records (~150-200 years) are
42 too short to fully sample modes of variability that are either rare or occur on multidecadal-to-
43 centennial timescales. This motivates the development of paleoclimatic proxy reconstructions,
44 which extends the observational baseline into the longer spectrum of climate variability and
45 provides a framework to consider both internal and forced climate changes.

46 Considerable advancements have recently been made in developing tree-ring
47 estimates of late Holocene hydroclimate variability across Scandinavia (Seftigen et al., 2014;
48 Cook et al., 2015). Being located in the high-latitude boreal zone, Scandinavia is well suited
49 for dendroclimatological studies and has a long tradition of climate and environmental
50 research using tree-ring data (Linderholm et al., 2010). The use of tree-ring proxy evidence to
51 study natural hydroclimate variability has however long been secondary when compared to
52 the scientific attention focused on providing local/regional reconstructions (Gunnarson et al.,
53 2011; Esper et al., 2012; McCarroll et al., 2013; Linderholm et al., 2014) and methodologies
54 (Björklund et al., 2012; 2014) to study temperature variability over the last several millennia.
55 Much of the tree-ring research at moisture-limited sites have until recently been limited to a
56 handful of exploratory papers (Helama and Lindholm, 2003; Linderholm et al., 2004; Jönsson
57 and Nilsson, 2009; Drobyshev et al., 2011; Seftigen et al., 2013) that generally develop one or
58 few chronologies to provide local precipitation/drought histories. These studies, together with
59 a steadily growing collection of high-latitude moisture sensitive tree-ring records (e.g.,
60 Seftigen et al., 2015), now serves as a basis for new possibilities to expand the detail and
61 accuracy with which the history of Northern European moisture conditions can be described.
62 A recent milestone in the field include the development of the “Old World Drought Atlas”
63 (“OWDA”, Cook et al., 2015), a set of tree-ring reconstructed year-to-year maps that provide
64 temporal *and* spatial details of droughts and wetness in the last millennium across Europe,

65 including Scandinavia. The OWDA has been used to elucidate hydroclimatic blueprints of the
66 Medieval Climate Anomaly (MCA, ~1000-1200 CE). Aligning with prior findings (Helama et
67 al., 2009), the atlas reveals the occurrence of so-called megadroughts in large portions of
68 continental north-central Europe and southern Scandinavia during the MCA period.
69 Interestingly, MCA and other “Old World” droughts seem to coincide with the timing of
70 some severe and persistent droughts documented in the climate history of North America.
71 While this suggests the presence of some common driving mechanisms across the North
72 Atlantic, being possibly related to variations in the Atlantic Ocean SST or/and the North
73 Atlantic Oscillation (Feng et al., 2011; Oglesby et al., 2012), the cause of these megadroughts
74 remains to be an open question.

75 While the proxy reconstructions undoubtedly play a pivotal role in unraveling
76 statistical qualities of past climate, they are, alone, not able to provide a comprehensive view
77 of the underlying physics governing the climate system. The forced-transient simulations over
78 the last millennium from fully coupled general circulation models (GCMs) (Taylor et al.,
79 2012) therefore offer an important complementary approach to the empirical analyses of
80 proxy estimates. Paleoclimate reconstructions provide an observational basis that spans
81 beyond current climate conditions that were used in developing and tuning such numerical
82 models, thus allowing for out-of-sample evaluations of the models’ predictive power. The
83 models, on the other hand, can be used to explore the dynamics that have driven climate
84 variability in the past.

85 This paper builds on previous tree-ring analyses (Seftigen et al., 2014; 2015) and
86 aims at employing a paleoclimate-data model comparison framework to further explore the
87 drivers and dynamics of drought/pluvials across Northern Europe. We analyze an ensemble of
88 six state-of-the-art GCMs from the Past Model Intercomparison Phase 3 (Schmidt et al., 2011
89 - PMIP3) and the Coupled Model Intercomparison Phase 5 (Taylor et al., 2012 - CMIP5) and
90 compare them to a new regional tree-ring-based proxy reconstruction of drought and wetness,
91 spanning the last millennium of the Common Era (CE). A combined data approach is used to
92 (1) evaluate to what extent the GCMs are capable in reproducing the key features of the
93 paleoclimate record, and (2) to estimate the role of external forcing versus internal variability
94 in driving the hydroclimatic changes regionally. The relative contribution of changes in
95 rainfall and surface temperature at inter-annual and decadal/longer time-scales to regional
96 hydroclimate patterns is also briefly explored, and the ability of the CMIP5/PMIP3 models to
97 simulate the mechanisms by which the regional hydroclimate is constrained by these two
98 variables are evaluated. The collective proxy-model data assessment will help to increase our

99 understanding of decadal/longer climate dynamics in regions and to evaluate the ability of the
100 state-of-the-art GCMs to simulate realistic future hydroclimatology regionally and across a
101 variety of different timescales.

102 The paper is structured as follows. Sect. 2 reviews the methods and describes the
103 paleoclimate and CMIP5/PMIP3 datasets. Subsequent analyses concentrates on comparing the
104 GCM simulations with the proxy based hydroclimate reconstructions (sect. 3), and delineating
105 the role of external (sect. 4) and internal (sect. 5) sources of variability over the last
106 millennium. The principal results and the implication of this study are discussed in sect. 6.

107 **2. Data and methods**

108 **2.1 CMIP5/PMIP3 simulations**

109 Simulations with six models (CESM1, CCSM4, IPSL-CM5A-LR, MIROC-ESM, MPI-ESM-
110 P, BCC-CSM1-1) contributing to the Coupled and Paleo Model Intercomparison Projects
111 Phases (CMIP3/PMIP3) (Schmidt et al., 2011; Taylor et al., 2012) have been used (Table I).
112 The analyses were restricted to models that have available complete monthly precipitation and
113 temperature variables spanning the last millennium (850-1849 CE) through historical (1850-
114 2005 CE) time intervals. The six millennium simulations were forced with reconstructed
115 solar, volcanic, greenhouse gas (GHG) and aerosol forcing, and partly land use changes,
116 whereas the historical simulations included natural and anthropogenic forcing (Schmidt et al.,
117 2011; Taylor et al., 2012). Except for CESM1, the analyses were limited to the first r1i1p1
118 ensemble member. Supplementary information (sect. S1, Fig. S1) provide an evaluation of six
119 selected model rainfall and temperature simulations against instrumental reference data
120 focusing on the northern European sector.

121 **2.2. Proxy data**

122 The use of annually resolved tree-ring series in the study of past hydroclimate variations has
123 traditionally been confined to lower-latitude arid and semi-arid region, with only a few
124 exceptions for the northern European sector. This is because the influence of moisture on tree-
125 growth generally decreases and is successively replaced by sensitivity to warm-season
126 temperature towards northern, cooler and wetter environment. Nevertheless, a growing body
127 of research (e.g., Helama and Lindholm, 2003; Wilson et al., 2012; Seftigen et al., 2013) has
128 established the potential to develop moisture-sensitive tree-ring chronologies in high-latitude
129 environments if a careful selection of species and sites is made. Building upon these findings,

130 we here analyse an existing network (Seftigen et al., 2014; 2015) of 25 *Pinus sylvestris* L.
131 tree-ring width chronologies from across a number of dry sites in southern Scandinavia (Fig.
132 1). The collected trees have typically been growing on well-drained soils or steep south-facing
133 slopes with warm and sunny exposure. Thus low soil moisture availability during the growing
134 season has been shown to be the most common growth-limiting factor in the tree-ring network
135 (Fig. S3 and S6).

136 The start dates of the chronologies varied across the collection, ranging from 532 to
137 1790 CE (Table II). All chronologies extended at least to year 1995. In order to reduce the
138 risk of natural/anthropogenic disturbance signal from inflicting non-climate noise upon the
139 reconstruction, the tree-ring data has been standardized in previous research (Seftigen et al.,
140 2014) by using a flexible “data-adaptive” method of standardization (Cook et al., 1995). This
141 has limited the degree to which longer-timescale climate information can be extracted.
142 Therefore, rather than using the already available hydroclimate reconstruction provided in
143 Seftigen et al. (2014), we have here re-processed the TRW collection with the newest signal-
144 free (SF) method of standardization (Melvin and Briffa, 2008), which has the capacity of
145 preserving long-term variability due to climate changes. The standardization was performed
146 with the ARSTAN software (Cook and Krusic, 2005). Chronologies combining living and
147 historical/subfossil material were standardized with a regional curve standardization (RCS)
148 approach (Briffa et al., 1992), applying a single RCS curve without any pith-offset
149 adjustments to detrend all series. To avoid spurious growth trends in the resulting RCS
150 chronologies stemming from a modern sample bias (Briffa and Melvin, 2011), tree-ring
151 datasets based only on living trees were standardized using the SF method in combination
152 with an age-dependent smoothing spline applied individually to each series. Prior to the
153 standardization, the modern chronology data were high-pass filtered and subsequently
154 grouped by means of a S-mode principal component analysis over the common interval (1792
155 – 1996 CE). The resulting eigenvector loadings are provided in supplemental material (Fig.
156 S2) and describe the major modes of high-frequency variability within the multiple modern
157 chronologies composing the dataset. The subdivision of the chronologies essentially identified
158 an east-west pattern, broadly corresponding to sub-regional differences in topography and
159 climate across the study domain. This suggested that the sub-regional tree-growth coherence
160 at high frequencies was driven by climate. Hence, it would be rational to expect a common,
161 climatically induced, growth variability also at the medium-frequency time scales, while any
162 disparities in the sub-regional tree-growth signal are likely mostly non-climatic in origin (i.e.
163 local site management practices, stand dynamics or other ‘random’ site-specific disturbances).

164 Therefore, in order to remove or minimize undesirable non-climatic noise upon our dataset,
165 modern tree-ring series were first merged group-wise as identified by the first four principal
166 components and subsequently detrended as four separate ‘batches’ using the SF method. The
167 standard version of the resulting tree-growth indices were subsequently separated and
168 averaged for each site to produce individual site chronologies. This procedure enabled us to
169 retain any shared, sub-regional, growth-forcing signal while removing site-specific medium-
170 to high-frequency noise.

171 Final data were adjusted to reduce the variance bias stemming from varying sample
172 size through time (Frank et al., 2006). The resulting chronologies were truncated where the
173 Expressed Population Signal (EPS) (Wigley et al., 1984) dropped below the 0.85 threshold,
174 or, in case of the longer chronologies, at year 1000 CE. The median segment length (MSL) of
175 all the chronologies (Table II) ranged between 74 and 357 years, and the median MSL across
176 all sites was 197 years. Although a precise quantification of returned frequency variance in
177 the final SF detrended tree-ring chronologies was not straightforward, the median MSL
178 suggested that it should be possible to use the network to reconstruct climate variability at
179 time scales up to ~200 years.

180 **2.3. Regional hydroclimatology**

181 The CMIP5/PMIP3 inter-model spread in spatial resolution and sophistication of soil
182 moisture schemes makes meaningful inter-model comparison difficult. To bypass some of
183 these challenges, the Standardized Precipitation Evapotranspiration Index (SPEI) (Vicente-
184 Serrano et al., 2013) was used to characterize the regional hydroclimatology across the study
185 domain. The SPEI, a commonly used metric of soil moisture balance, has successfully been
186 used as a target variable in several prior tree-ring reconstructions (e.g., Seftigen et al., 2014;
187 2015). The index is not a state variable but rather an offline metric of the surface moisture
188 balance that can be consistently derived across models and therefore provide standard
189 measure of hydroclimatic variability across GCMs. The computation of the index is based on
190 normalized monthly climatic water balance, i.e. cumulative precipitation minus potential
191 evapotranspiration (PET), summed over multiple time scales and computed as standard
192 deviations with respect to long-term mean (Vicente-Serrano et al., 2010). The PET was here
193 estimated with the Thornthwaite approach (Thornthwaite, 1948). The method requires surface
194 temperature and latitude data only, and has therefore frequently been used for PET
195 computations over the historical period. Moreover, the choice of methods is motivated by the
196 larger confidence that is placed on GCM simulations of temperature compared to other

197 variables (vapor pressure, wind speed, net radiation, etc.) that are required for more physically
198 based parameterizations of PET. At each grid point, model SPEI were derived from estimated
199 PET and simulated rainfall over the past1000 and historical periods and then standardized
200 against the 1901-2005 normalization period using the SPEI R package version 1.6 (Vicente-
201 Serrano et al., 2010).

202 The proxy dataset was generated by a point-by-point regression (PPR) methodology
203 that was applied to the TRW network to produce a SPEI reconstruction spanning the past
204 millennium. The climate field reconstruction method is based on principal component
205 regression procedure using the TRW chronologies as potential predictors to develop a set of
206 nested multivariate stepwise regression models (see Cook et al., 1999 for details). Here we
207 employed the same calibration/validation scheme, predictor selection and pre-processing steps
208 as previously described in (Seftigen et al., 2015). We performed a full period calibration over
209 the 1901-1995 period of TRW/climate data overlap. A conventional split period
210 calibration/validation procedure was additionally performed for an independent validation of
211 the SPEI estimate, by splitting the full calibration period into two periods of roughly equal
212 length (1901-1948 and 1949-1995 periods) and computing/comparing validation metrics over
213 both periods. Each nest was centered and scaled to have the same mean and variance as the
214 observational data in the calibration period. The instrumental SPEI target field for the
215 reconstruction was computed from the CRU TS 3.22 (Harris et al., 2014) 0.5° latitude x 0.5°
216 longitude gridded rainfall and temperature datasets over the southern portion of Scandinavia
217 ($55^\circ - 65^\circ$ N and $5^\circ - 30^\circ$ E) (Fig. 1), using the same conventions as described above. Simple
218 correlation analysis conclusively demonstrated a short-term early summer moisture sensitivity
219 of the TRW records over most of the study domain (Fig. S3). Based on these findings, we
220 selected June SPEI, aggregated over a 2-month time scale, as the target season data for the
221 reconstruction. A final regional time series was averaged from grid points where the
222 calibration regression models explained at least 20% of instrumental variance and the
223 reduction of error (RE) and coefficient of efficiency (CE) (National Research Council, 2006)
224 verifications metrics exceeded the generally accepted threshold value of zero across all nests
225 ($N = 521$ grid points). The mean tree-ring hydroclimate reconstruction (henceforth ScandH17)
226 and the corresponding instrumental target dataset are shown in Fig. 1, and a validation of the
227 reconstruction against 20th century instrumental data that have been withheld from the
228 calibration is provided in supplementary materials (Fig. S4). Results are variable depending
229 on the calibration/validation period used; the validation/calibration statistics are generally
230 stronger for the 1901-1948 period and substantially weaker for the 1949-1995 period. The

231 most recent and well-replicated nests (mid-1600s to present) are generally explaining the
232 greatest amount of instrumental variance ($R^2 > 40\%$ for the majority of the grid points). A
233 loss of grid cells with declining proxy availability and a drop in reconstruction skill is
234 occurring prior to the late-1400s and subsequently in the 1200s. Point-wise correlation with
235 gridded instrumental SPEI dataset shows that ScandH17 is representative for a larger area in
236 southern and central Scandinavia with a correlation ‘hot spot’ exceeding 0.6 (Fig. 1).

237 **2.4. Analyses**

238 The new proxy-based reconstruction was used to assess the temporal evolution of droughts
239 and pluvials over the last millennium and to elucidate the mechanisms that govern
240 hydroclimate changes in the northern European sector ranging from interannual to
241 multidecadal time scales. We briefly analyze the relative role of temperature (which
242 modulates potential evapotranspiration) and precipitation (which supplies moisture) in
243 regional hydroclimate variability (sect. 5). We use the last-millennium and historical
244 CMIP5/PMIP3 simulations of temperature and precipitation. As there are no independent,
245 annually resolved, proxy reconstructions of rainfall variability currently available for the
246 region, we only included temperature estimates in the analyses of ScandH17. For this
247 purpose, the previously published Linderholm et al. (2014) (hereafter ScandT14) summer
248 temperature reconstruction was used. The two reconstructions ScandH17 and ScandT14 share
249 no common predictors and are thus fully independent, which ensures that any circular
250 statement in the comparison can be ruled out. The ScandT14 record is based on tree-ring
251 maximum density (MXD) and blue intensity data from central-northern Scandinavia and is in
252 terms of signal strength and preserved multi-centennial scale variability one of the best
253 temperature reconstructions currently available for the region.

254 Furthermore, we extended our analyses to the model domain using the methodology
255 of paleoclimate data-model comparison. There were three main components to the combined
256 approach. Firstly, we evaluated the consistency in various datasets and assessed whether the
257 CMIP5/PMIP3 simulations have similar statistical properties as the reconstruction (sect. 3).
258 Spectral and spectral coherency analyses were performed in two ways. The first is the multi-
259 taper approach (Thomson, 1982) based on 4 tapers, where a Monte-Carlo procedure is used to
260 estimate phase 95% confidence limits. We also used the wavelet cohere analyses available in
261 the Grinsted et al. (2004) MATLAB package to assess the frequency dependent relationships
262 and phasing between various datasets.

263 Secondly, we used the Superposed Epoch Analysis (SEA) (Haurwitz and Brier,
264 1981) to evaluate the influence of volcanic aerosol forcing on hydroclimate, temperature and
265 precipitation of the Scandinavian region at inter-annual time scales (sect. 4). For the last
266 millennium, monthly mean volcanic forcing series were obtained from three different sources:
267 Gao et al. (2008), Crowley and Unterman (2013) and Sigl et al. (2015) datasets. We note that
268 the former two forcings have been used as the boundary conditions for the last millennium
269 CMIP5/PMIP3 simulations. The length of the proxy and model data allowed us to include sets
270 of the 20 largest eruptions since 1100 CE (Table III) from the annual forcing series to assess
271 the mean response. For each series and eruption, anomalies for ten post-eruption years were
272 computed relative to a five-year pre-eruption mean. The confidence intervals around the
273 composite responses were determined using a Monte Carlo block resampling ($N = 10\,000$) of
274 the actual event year windows (see Adams et al., 2003 for details).

275 Thirdly, we evaluated the skill of the models to represent the dynamics that drive the
276 variability in hydroclimate of the Scandinavian region by establishing a link between
277 simulated and reconstructed SPEI series and fields of mean sea level pressure (MSLP) over
278 the Atlantic-European sector (sect. 5). Grid point correlations were computed to assess the
279 spatial features and the strength of the teleconnections patterns over the modern era (1950-
280 2005 CE). The analysis was also extended over the last millennium (1000-1849 CE) to
281 investigate the nature of teleconnection stability without the influence of anthropogenic
282 forcing. The gridded monthly instrumental HadSLP2 dataset spanning 1850-present (Allan
283 and Ansell, 2006) was used for comparison with observed and proxy-based estimates of
284 hydroclimate.

285 **3. Modeled and reconstructed hydroclimate series**

286 The regional warm season hydroclimate variability averaged across the six CMIP5/PMIP3
287 models together with the new ScandH17 proxy reconstruction over the last millennium are
288 shown in Fig. 2a-b. Individual model SPEI time series are displayed in Fig. 2c-h. All data
289 have been normalized and centred over the common interval from 1000 to 1995 CE, since this
290 first joint proxy-model comparison focuses on the common relative changes rather than on the
291 magnitude and the absolute values. A simple visual comparison reveals that the models and
292 the reconstruction have generally little agreement in the variance structure and trends. The
293 reconstruction is dominated by a large decadal-to-multidecadal variability while the
294 multimodel mean is relatively flat at these time scales. There are some common features in
295 some of the GCMs and the proxy datasets though (Fig. 2c-h), e.g., the drying in the 19th

296 century, but these are rare when the full millennium is considered and are likely occurring by
297 chance. The historical interval in the proxy record is characterized by a drought in the mid-
298 1800s and a gradual increase in wetness over the 20th century, while, with the exception of
299 short dry episode in the early-1900s, there is no long-term trend in the multimodel mean over
300 the modern era.

301 The very low correlation at inter-annual time scales is to be expected, as the internal
302 variations in the various records represent different realizations of the climate system, which
303 is to a very large extent chaotic at that time scale. The response of each ensemble member to a
304 strong external forcing applied to the model would nevertheless ideally agree (i.e. external
305 punctual perturbations such as volcanic eruptions could induce a coherent short-term
306 response, see sect. 4). Averaging across models or over multiple ensemble members will
307 reduce the contribution from stochastic variability so that the remaining signal can come
308 closer to the model response to external forcing. The comparison between ScandH17 and the
309 multimodel assemble mean reveal, however, no statistically significant agreement between
310 the series, neither on the interannual nor on decadal timescales, suggesting that the simulated
311 hydroclimate changes are not strongly tied to exogenous forcing. Moreover, we found no
312 statistically significant correlation between the different ensemble members in the same
313 model (CESM1) (Fig. 2c), which is the only model providing multiple ensemble members
314 (the only difference among these being the air temperature at the start of each ensemble
315 member (Otto-Bliesner et al., 2016) over the historical and past millennium intervals). The
316 poor overlap between CESM1 ensemble members as well as the individual GCM simulations
317 over the past millennium (despite the use of largely similar forcing series to drive the
318 simulations) is indicative of a larger contribution from internal variability on simulated
319 drought/pluvial occurrence than from changes in exogenous forcing.

320 We compare the spectral properties of the six individual CMIP5/PMIP3 models to
321 the ScandH17 reconstruction and observational data, which allows for a general evaluation of
322 potential frequency biases. Results indicate that the underlying spectrum of reconstructed
323 hydroclimate variability is significantly redder on decadal-centennial timescales than
324 indicated by the simulated SPEI (Fig. 3a and 3d), as has previously been noted (Ault et al.,
325 2012; Ault et al., 2013). In contrast, more hydroclimate variance is concentrated on
326 interannual timescales in the CMIP5/PMIP3 archive than in ScandH17 reconstruction. At
327 frequency bands < 8 years, the power spectral range of most models is systematically above
328 the confidence interval of ScandH17. We also consider the agreement between simulated,
329 reconstructed (ScandT14) and instrumental temperature data in terms of their spectral

330 properties (Fig. 3b). Although the degree of agreement is higher than for hydroclimatology
331 and most models lie within the reconstruction confidence bands (see also sect. S2
332 supplementary materials), there are some models that have more variance than the
333 reconstruction at periods < 10 years.

334 **4. The role of volcanic forcing**

335 Large explosive volcanic eruptions are an important natural radiative forcing mechanism at
336 timescales ranging from seasons to decades (Shindell et al., 2004; Gleckler et al., 2006). The
337 imposed perturbation on the climate system by such events will depend on the nature of the
338 eruption, the magnitude of change in the energy entering the earth's atmosphere, the
339 background climate and internal variability, latitude and season. Analysis of observational
340 data (Shindell et al., 2004), tree-ring records (D'Arrigo et al., 2013) and model simulations
341 (Anchukaitis et al., 2010) indicate a considerable spatial variability in the dynamical response
342 of the climate system to volcanic forcing, with some regions experience surface and
343 tropospheric cooling effects and other regions showing no significant change or even
344 warming effect. Here, we assess the magnitude and timing of Scandinavian summer
345 temperature, rainfall and hydroclimate response to short-term radiative cooling due to
346 volcanic aerosols.

347 A peak cooling is observed one year after the eruption, both in ScandT14 and in the
348 CMIP5/PMIP3 composite average, for all the three forcings considered (Fig. 4). In addition,
349 there is a significant cooling in the year of the event for the Crowley and Unterman (2013)
350 and Sigl et al. (2015) lists. ScandT14 reveal a marginally greater cooling (2.0 °C, mean of the
351 three event lists) than the model average (1.8 °C) one year after the eruption. Remarkably,
352 there is a high degree of similarity in the proxy and in the GCMs not only in terms of the
353 signal timing and the magnitude of the cooling response, but also the rate of recovery. A
354 complete recovery after the volcanic cooling is found two years after the eruption,
355 independent of the forcing list. These results are generally consistent with prior studies
356 (Fischer et al., 2007; Jones et al., 2013; McCarroll et al., 2013) highlighting the importance of
357 explosive volcanism as an external driver of Northern European temperature variability. They
358 also provide a relevant test of the model to radiation perturbations. The agreement between
359 the model simulations and proxy data demonstrates the credibility of the models.

360 Existing research on the response of high-latitude rainfall and hydroclimate to
361 volcanism is limited (in part because high resolution moisture sensitive proxy records are
362 sparse or unavailable). Fischer et al. (2007) found a weak tendency to drying conditions over

363 southern/central Scandinavia in the summer of year 0 and year 1 after the eruption.
364 Circulation changes to the surface cooling were shown to modulate the directly forced
365 response. On continental and global scales, both observational and modeling studies have
366 found a decrease in precipitation (Iles et al., 2013) and streamflow (Iles and Hegerl, 2015) in
367 response to large explosive eruptions, particularly in climatologically humid regions (Carley
368 and Gabriele, 2014). The short-term drying is caused by a reduction in incoming solar
369 radiation reaching the surface, which reduces evaporation, whilst the widespread cooling
370 stabilized the atmosphere and lowers its water holding capacity (Bala et al., 2008). Here, we
371 apply SEA on ScandH17 and simulated SPEI and precipitation to examine the influence of
372 volcanism on Scandinavian moisture availability. A statistically significant reduction in
373 simulated rainfall is observed for all event lists, ranging between the year of the event
374 (Crowley and Unterman, 2013 dataset) and up to two years (Sigl et al., 2015 dataset)
375 following the eruption. We find, however, that the precipitation signal is less consistent across
376 the six CMIP5/PMIP3 models than the cooling effect observed in the simulated temperature
377 series.

378 The SEA on SPEI time series reveals a statistically significant drying after large
379 volcanism. However, the response is more muted than the response of temperature and
380 rainfall separately. Moreover, the agreement between proxy data and the model composite
381 average is weak and there are large inconsistencies between the different forcing records.
382 ScandH17 show a progressive transition from wet conditions in the event year and preceding
383 years to dryer conditions in the consecutive years with significant dry anomalies five
384 (Crowley and Unterman, 2013 dataset) and seven years (Sigl et al., 2015; Gao et al., 2008
385 datasets) after the perturbation. For the CMIP5/PMIP3 multimodel multi-eruption average,
386 only the fifth year after the eruption (Crowley and Unterman, 2013 list) is found to be
387 significantly drier than the adjacent years.

388 The observed weak influence of volcanic forcing on the hydroclimate of the region
389 can be explained by various factors. For example, our results reveal that GCM simulated post-
390 volcanic cooling remains significant for about two years and matches the timescale of the
391 post-volcanic rainfall decrease. Since the SPEI accounts for both supply and demand changes,
392 the net effect would be such that the temperature-driven PET decrease counter a substantial
393 fraction of the precipitation-driven drying, thus producing SPEI values near neutral.
394 Furthermore, the muted response of ScandH17 may arise from autocorrelated biological
395 memory in the TRW data (Esper et al., 2015). The high year-to-year persistence may bias its
396 ability to estimate the abruptness and severity of climatic extremes caused by volcanic

397 cooling. The tree-ring MXD and the blue intensity parameters have, in contrast, been
398 suggested to be superior to TRW for recording short term climate perturbations (Wilson et al.,
399 2016), which is likely the reason why the response of ScandT14 is more immediate than that
400 of ScandH17.

401 **5. Internal sources of variability**

402 If the regional hydroclimate variability is indeed dominated by internally generated stochastic
403 components of variability (see sect. 3), atmospheric circulation changes can be the key
404 process shaping regional patterns of moisture availability. Advancing our understanding of
405 the range, stability and strength of teleconnection behavior (defined here as the correlation
406 between hydroclimate and MSLP over the Atlantic-European sector) and its coupling to
407 regional hydroclimate would provide an improved understanding of drought/pluvial dynamics
408 and associated uncertainty. In this section, we first explore major modes of atmosphere
409 variability that impact summertime northern European hydroclimatology. We also assess
410 more extensively the contribution of atmospheric processes (and possible land-atmosphere
411 interactions) by investigating the couplings between hydroclimate and arguably the two most
412 critical variables of the terrestrial climate and the hydrological cycle: precipitation and
413 temperature.

414 To determine the role of teleconnections, correlation of MSLP fields with the
415 hydroclimatic variables over the recent 50 years of the post-industrial era were computed.
416 Results are shown in Fig. 5. As expected, we find that atmospheric dynamics have a
417 significant role in climate variability in the region: a strong correlation with regional
418 hydroclimate is found when MSLP in concurrent months (i.e. May-June) is considered. The
419 results show that the proxy based and CMIP5/PMIP3 simulated dynamics are largely
420 consistent with those in the instrumental record, indicating that both the proxy and the models
421 contain to some degree realistic teleconnections. A consistent feature across the datasets is a
422 tripole structure that would favor increased moisture supply into the Scandinavian region. The
423 structure is characterized by anomalous cyclonic conditions across Scandinavia and high-
424 pressure systems extending over Iceland-Greenland and, albeit less pronounced, over
425 European Russia - Central Asia. Out of the six CMIP5/PMIP3 models, MIROC-ESM is the
426 one showing the largest discrepancy with the major spatial features of the observed
427 correlation map, by failing to reproduce the anti-cyclonic pattern over Iceland-Greenland.
428 Additionally, MIROC-ESM and also CCSM4 show a meridional and zonal shift of the
429 European Russia - Central Asia high-pressure structure towards the Mediterranean region.

430 Atmospheric circulation has been identified as key contributor to recent changes in
431 the climate of Europe in both summer and winter (van Oldenborgh and Van Ulden, 2003;
432 Jones and Lister, 2009). To assess the stationarity of observed MSLP patterns, the analysis
433 was repeated for the pre-industrial last millennium (1000-1849 CE) period (Fig. 6). The
434 exercise was restricted to five GCMs for which simulated MSLP was available for the pre-
435 industrial era (BCC-CSM1-1 was not included). The simulated dynamical relationships were
436 found to be largely stable for all five models, being consistent with observed correlations
437 patterns in the modern era. This suggests a weak influence of anthropogenic forcing on the
438 structure of the dynamical drivers of Scandinavian hydroclimate. In addition to raw data,
439 correlation analysis with 10-year low-passed data was also completed for the pre-industrial
440 period with the purpose to elucidate the drivers of multidecadal hydroclimate variability. We
441 find similar, yet weaker, correlation patterns as compared to the high-frequency variations
442 (results not shown).

443 Precipitation and temperature are the two key variables of the hydrological cycle.
444 Assessing the relative contribution of these two variables to the surface moisture balance
445 across various timescales, and the mechanisms that control and modulate it, is therefore of
446 great interest to the study of regional processes on surface energy and water budgets. While
447 past studies have investigated the relationship between temperature, moisture supply and
448 drought in various regions on daily, seasonal and interannual timescales (Adler et al., 2008;
449 Berg et al., 2015; Trenberth, 2011; Madden and Williams, 1978), the nature of concurrent
450 multidecadal/ long-term relationship is still far from being clear. A joint analyses of the new
451 hydroclimate reconstruction with the recently published Linderholm et al. (2014- ScandT14)
452 fully independent warm-season temperature record for Scandinavia is provided in Figs. 7 and
453 8, in conjunction with the CMIP5/PMIP3 simulations of temperature, rainfall and SPEI. On
454 interannual timescales, five out of six GCMs show a significant ($p < 0.05$) negative
455 association between simulated interannual temperature and rainfall, with correlation
456 coefficients ranging between $r = -0.12$ and -0.29 (1000-2005 CE period). Moreover, all model
457 show a strong negative (positive) correlation between temperature (precipitation) and SPEI in
458 the last millennium, ranging between $r = -0.63$ and -0.80 ($r = 0.61$ and 0.84). Extending the
459 analysis to the instrumental data, we find that the regional year-to-year variability in
460 hydroclimate is more closely organized around changes in precipitation than changes in
461 temperature (Fig. S5). In southern Scandinavia, weak negative correlations appear between
462 temperature and rainfall (Fig. S5a), and temperature and SPEI (Fig. S5b). Over northern
463 Scandinavia, the interannual correlations are not significant.

464 Turning to the tree-ring records, we find no significant relationship between
465 ScandH17 and ScandT14 reconstructions on a year-to-year basis ($r = 0.01$ and $p = 0.8$ on first
466 difference data, 1100-1995 CE period). The considerable distance separating the sampling
467 sites of each tree-ring collection, and the fact that summer precipitation occurrence often
468 depends on local processes and moisture fluxes could explain the lack of a shared annual
469 signal. Notably, however, we find that the two reconstructions are mostly in phase on decadal
470 and longer timescales ($r = 0.30$ and $p < 0.001$ on loess-smoothed data, 1100-1995 CE period)
471 (Fig. 7), suggesting that the low-frequency temperature and hydroclimate variability is more
472 spatially coherent. These results are corroborated by the cross-wavelet coherency analysis
473 (Fig. 8a), revealing that the ScandH17 and ScandT14 reconstructions share significant ($p <$
474 0.05) in phase variance in multidecadal frequency throughout most of the last millennium.
475 The coupling seems to arise from overlap in shared frequencies at wavelengths longer than \sim
476 50 years (c.f. Fig. 3). Interestingly, we find that the paleoclimatic evidence and the
477 CMIP5/PMIP3 models portray a considerably different response of hydroclimate in
478 Scandinavia to long-term temperature changes. While the proxy time series suggests that
479 prolonged wet periods generally coincide with elevated temperatures, the majority of the
480 CMIP5/PMIP3 models indicate that warm decades should have been dryer (Fig. 8b – h and
481 Fig. S9).

482 Instrumental and paleoclimate evidence collectively suggest a time-dependent shift
483 of the relationship between regional temperature and hydroclimate, which in turn implies that
484 different mechanisms governing the climate system might be operating at high (interannual)
485 and low (decadal/longer) frequencies, respectively. The previously discussed strong link
486 between inter-annual regional hydroclimate variability and atmospheric pressure patterns
487 indicates that atmospheric dynamics is likely a dominant driver of hydroclimate in the
488 northern European sector on interannual basis. The inverse covariability between warm-
489 season temperature and moisture supply, which is revealed by the instrumental record, may
490 arise from synoptic-scale correspondence between reduced cloud cover/rainfall and increased
491 incoming shortwave radiation warming the surface during clear sky conditions. In addition,
492 soil moisture exert a strong influence on the allocation of available energy between latent and
493 sensible heating, especially in the warm-season (Seneviratne et al., 2010). Reduced soil
494 moisture, for example, is associated with reduced latent heat flux and thus increased sensible
495 heating and higher air temperatures near the surface. Resulting positive feedbacks of a
496 modified surface heat flux partitioning on cloud cover and radiation (Gentine et al., 2013) and

497 large-scale circulation (Haarsma et al., 2009) could further strengthen the influence of rainfall
498 variability on the thermal climate.

499 The positive association between temperature and SPEI that is found in the proxy
500 records on decadal-to-multidecadal timescales could imply that the long-term regional
501 hydroclimate variability is more sensitive to changes in moisture supply (precipitation) rather
502 than to increased evaporative demand due to warming. It may also suggest that the regional
503 moisture balance might be favored by the Clausius-Clapeyron relation (Allen and Ingram,
504 2002), prescribing an increase in rainfall and intensity of the hydrological cycle during
505 warmer periods in the past millennium. This is generally referred to as ‘wet-get-wetter’/‘dry-
506 get-drier’ mechanism and is attributed to thermodynamic processes (Held and Soden, 2006).
507 In the absence of changes in atmospheric circulation, changes in net moisture supply with
508 warming are related to change in moisture content of the atmosphere. It presupposes that
509 existing circulations will transport more moisture into mesic regions of the globe (e.g., tropics
510 and the mid- to latitudes of Northern Hemisphere), whilst dry regions (e.g., subtropics) will
511 get even dryer, with the fractional change determined by Clausius-Clapeyron relation. In
512 contrast to the proxy records, the model composite average reveals a twentieth-century
513 temperature and rainfall increase yet little change in hydroclimate (Fig. 7b). The multimodel
514 assessment implies that natural variability plays only a subsidiary role in recent changes and
515 that forcing from anthropogenic greenhouse gases (GHG) may have played a more important
516 role (as previously discussed, the effect of GHG-forcing on interannual teleconnection
517 patterns in the modern era seems to be weak). Moreover, the absence of any significant trend
518 in simulated SPEI series indicates that the gains in moisture from increased precipitation are
519 large enough to compensate for any GHG-induced increase in PET in the post-industrial
520 period.

521 **6. Summary and discussion**

522 This study presents the first comprehensive assessment of past variability and trends in
523 hydroclimate of northern European sector over the last millennium of the Common Era along
524 with interrelated variables: precipitation, which supplies moisture, and temperature, which
525 modulates evapotranspiration. A combined approach comparing observational (both
526 instrumental and proxy based) and model-based results is used for evaluation of simulated
527 and real-world interannual-to-centennial climate variability and the underlying physics
528 governing the climate system. A number of important findings emerge from the collective
529 comparison:

530 [1] Models and proxy data are found to broadly agree on the modes of atmospheric variability
531 (sect. 5) that produces droughts and pluvials in Scandinavia. Despite these dynamical
532 similarities, large discrepancies between model simulations and the proxy reconstruction are
533 shown to exist. The droughts and pluvials in the forced simulation are not temporally
534 synchronous with those in the proxy record, nor do the GCM spectra agree with the proxy
535 spectra on the amount of variance present on short and long timescales (sect. 3).

536 [2] The proxy data and the CMIP5/PMIP3 models reveal different effects of long-term
537 temperature changes on summer hydroclimate in Scandinavia. According to the GCMs,
538 prolonged droughts generally coincide with elevated temperatures. The proxy evidence, on
539 the other hand, suggests that warm decades in the last millennium also tend to be wet decades.
540 Although the precise reason for the model-proxy mismatch remains to be unraveled, our
541 results suggests that spectral inconsistencies among the model and proxy datasets could be
542 one possible explanation for the mismatch.

543 [3] There are considerable disagreements among hydroclimate features shown by the
544 CMIP5/PMIP3 simulations (despite the use of largely similar forcing series) (sect. 3).
545 Together, these results point to the possibilities of dominant influence of stochastic processes
546 for the regional hydroclimate and/or deficiencies in the models to realistically represent
547 relevant processes in reality.

548 Most notably we find clear inconsistencies between the paleoclimate record and the
549 model spectra. At multidecadal/longer timescale there is more variability in the proxy data
550 than in the models. In contrast, the dominance of GCM simulated interannual components of
551 variability is not reflected in the proxy record. It is difficult to determine explicitly whether it
552 is an external forcing or internal sources that drive the decadal and longer variance in the
553 proxy reconstruction. Prior studies have highlighted the importance of external influences on
554 regional climate variability at different timescales (e.g., Gleckler et al., 2006; Thiéblemont et
555 al., 2015; Sigl et al., 2015). Although we find a short term response of regional hydroclimate
556 to volcanic perturbations (sect. 4), multi-year anomalies in the proxy reconstruction do,
557 however, not appear to correspond well with the epochs following the large volcanic
558 eruptions (e.g., in the 1250s, 1450s and 1810s) used to force the models. Thus we cannot rule
559 out that the variability in the reconstruction largely arise from internal sources of variation.
560 Consequently, if the proxy-inferred decadal-to-multidecadal variability is accurate and if the
561 variability is indeed largely unforced, then its magnitude is well beyond what any of the
562 current generation global climate models are able to produce in the region. Underestimation
563 of redness in the models on multidecadal/longer timescales, suggests the GCMs might be

564 lacking/underestimating processes important to the variability at these timescales. There are a
565 number of recognized limitations relating to the dynamics that are relevant to the climatology
566 of the North Atlantic-European sectors. One such example is that models have generally been
567 unable to simulate low-frequency variability in the North Atlantic Oscillation (Osborn, 2004).
568 They have also been shown to underestimate the periodicity of the Atlantic Multidecadal
569 Oscillation (Kavvada et al., 2013), which has implications for the associated hydroclimate
570 impact on neighboring continents (Coats et al., 2015). If, on the other hand, the proxy
571 estimated multidecadal/longer variability in the last millennium is forced by exogenous
572 mechanisms, then either 1) it is a forcing component that is largely missing in the
573 CMIP5/PMIP3 models, alternatively, 2) it is a forcing component that generates a different
574 long-term response in the models compared to the “proxy view” of regional
575 hydroclimatology.

576 It is not possible to pinpoint which part of the disagreement between models and the
577 proxy comes from uncertainties in the tree-ring reconstruction, deficiencies in the forcing
578 series used to drive the models, or from deficiencies in the model. Our analyses have included
579 precipitation simulation – a challenging variable for GCMs to simulate accurately. The coarse
580 spatial resolution of the models gives only an approximate representation of the topographic
581 features, which are important for regional hydroclimate. Another possibility is that the scale
582 of the GCMs is unrepresentative of the point estimate provided by the ScandH17
583 reconstruction. On the other hand, the mismatch between grid box and point estimates is
584 expected to reduce at longer timescales (Jones et al., 1997). There are also limitations of the
585 tree-ring proxy and uncertainties in the interpretation of the data that cannot be ignored. Tree-
586 rings and other biological archives may integrate climate conditions over multiple years
587 (Zhang et al., 2015), which could potentially overestimating the ratio of low to high frequency
588 variability (Franke et al., 2013). While we have been able to establish that prevailing summer
589 moisture availability has been the main growth limitation of trees in the ScandH17 network
590 on an interannual basis over the twentieth century (Figs. S3 and S6), we cannot verify the
591 drought-tree growth model in the pre-instrumental era or across longer spectrum of
592 variability. We are not able to rule out that there might have been climatic regimes in the past
593 that would have caused dynamical shift in the tree growth response to climate, and potentially
594 have called into question the uniformitarian paradigm traditionally applied in the field of
595 dendroclimatology. These non-stationaries may include frequency dependent sensitivity of the
596 proxy system to climate. While we are able to show that the year-to-year variability of growth
597 is dominated by a moisture signal, the impact of growing season temperature on lower

598 frequency variations has yet to be established. In addition to these issues, there are also risks
599 that less well know dynamics outside the climate system may introduce variability into the
600 records at decadal/longer timescales. Advances in the mechanistic understanding of the
601 various proxies and the processes through which they record environmental change, e.g.,
602 through development and refinement of process-based forward models (Tolwinski-Ward et
603 al., 2011), is currently an emerging priority in the field.

604 The discrepancies in CMIP5/PMIP3 simulated and proxy reconstructed hydroclimate
605 variability in the last millennium is an issue that must be addressed when assessing
606 projections of future hydroclimate change. The lack of adequate understanding for
607 mechanisms linking temperature and moisture supply on longer timescales has important
608 implication for future projections. Weak multidecadal variability in models also implies that
609 inference about future persistent droughts and pluvials based on the latest generation global
610 climate models will likely underestimate the true risk of these events. Reconciliations for the
611 apparent proxy – model mismatch will require efforts from the proxy, modeling and statistics
612 groups, including additional proxy records and refined model simulations of hydroclimate
613 variability in the last millennium, together with the development of alternative approaches for
614 joint proxy-model assessments. Having here provided a first comparison of reconstructed and
615 simulated hydroclimate for Scandinavia, our future efforts will include adaptations of the data
616 assimilation approach to paleoclimate reconstruction. Such efforts hold promise for reducing
617 the uncertainties associated with model physics, external forcings, and internal climate
618 variability, and ultimately help to refine our view of past and future hydroclimate changes.

619 **Data availability**

620 Individual unprocessed tree-ring series can be downloaded from the International Tree-Ring
621 Data Bank (<http://www.ncdc.noaa.gov/paleo/treering.html>), the SAIMA Tree-Ring Data Bank
622 (<http://lustiag.pp.fi/Saima/dendrotieto.htm>), or from the supplement (see Table II). The
623 CMIP5/PMIP3 climate model output can be obtained though the Earth System Grid - Center
624 for Enabling Technologies (ESG-CET) portal (<http://pcmdi9.llnl.gov/>). The ScandT14
625 temperature reconstruction is archived through the NOAA paleoclimate database
626 (<https://www.ncdc.noaa.gov/paleo/study/22692>). The ScandH17 reconstruction and all signal-
627 free standardized tree-ring chronologies are provided in the supporting information.

628 **Acknowledgments**

629 K. Seftigen was supported by the FORMAS mobility starting grant for young researchers
630 (grant # 2014-723). H. Goosse is senior research associate with the FRS/FNRS, Belgium. The
631 authors wish to acknowledge the researchers who have produced and made their tree-ring
632 chronologies available. The authors also wish to thank the World Climate Research
633 Programme's Working Group on Coupled Modelling, which is responsible for CMIP, and to
634 acknowledge the climate modeling groups (listed in Table I of this paper) for producing and
635 making available their model output. For CMIP the U.S. Department of Energy's Program for
636 Climate Model Diagnosis and Intercomparison provides coordinating support and led
637 development of software infrastructure in partnership with the Global Organization for Earth
638 System Science Portals. The authors also wish to acknowledge Editor Dr Helen McGregor, 2k
639 Special Issue Data Review Team, and two anonymous reviewers for comments on this paper.

640 **References**

- 641 Adams, B. J., Mann, M. E., and Ammann, C. M.: Proxy evidence for an El Nino-like response to
642 volcanic forcing, *Nature*, 426, 274-278, 2003.
- 643 Adler, R. F., Gu, G., Wang, J.-J., Huffman, G. J., Curtis, S., and Bolvin, D.: Relationships between
644 global precipitation and surface temperature on interannual and longer timescales (1979–2006),
645 *Journal of Geophysical Research*, 113, 10.1029/2008jd010536, 2008.
- 646 Allan, R., and Ansell, T.: A New Globally Complete Monthly Historical Gridded Mean Sea Level
647 Pressure Dataset (HadSLP2): 1850–2004, *Journal of Climate*, 19, 5816-5842, 10.1175/jcli3937.1,
648 2006.
- 649 Allen, M. R., and Ingram, W. J.: Constraints on future changes in climate and the hydrologic cycle,
650 *Nature*, 419, 224-232, 2002.
- 651 Anchukaitis, K. J., Buckley, B. M., Cook, E. R., Cook, B. I., D'Arrigo, R. D., and Ammann, C. M.:
652 Influence of volcanic eruptions on the climate of the Asian monsoon region, *Geophysical Research*
653 *Letters*, 37, n/a-n/a, 10.1029/2010gl044843, 2010.
- 654 Ault, T. R., Cole, J. E., and St. George, S.: The amplitude of decadal to multidecadal variability in
655 precipitation simulated by state-of-the-art climate models, *Geophysical Research Letters*, 39, n/a-n/a,
656 10.1029/2012gl053424, 2012.
- 657 Ault, T. R., Cole, J. E., Overpeck, J. T., Pederson, G. T., St. George, S., Otto-Bliesner, B.,
658 Woodhouse, C. A., and Deser, C.: The Continuum of Hydroclimate Variability in Western North
659 America during the Last Millennium, *Journal of Climate*, 26, 5863-5878, 10.1175/jcli-d-11-00732.1,
660 2013.
- 661 Bala, G., Duffy, P. B., and Taylor, K. E.: Impact of geoengineering schemes on the global
662 hydrological cycle, *Proceedings of the National Academy of Sciences*, 105, 7664-7669,
663 10.1073/pnas.0711648105, 2008.
- 664 Berg, A., Lintner, B. R., Findell, K., Seneviratne, S. I., van den Hurk, B., Ducharne, A., Chéruy, F.,
665 Hagemann, S., Lawrence, D. M., Malyshev, S., Meier, A., and Gentine, P.: Interannual Coupling
666 between Summertime Surface Temperature and Precipitation over Land: Processes and Implications
667 for Climate Change*, *Journal of Climate*, 28, 1308-1328, 10.1175/jcli-d-14-00324.1, 2015.
- 668 Björklund, J., Gunnarson, B. E., Krusic, P. J., Grudd, H., Josefsson, T., Östlund, L., and Linderholm,
669 H. W.: Advances towards improved low-frequency tree-ring reconstructions, using an updated *Pinus*
670 *sylvestris* L. MXD network from the Scandinavian Mountains, *Theor Appl Climatol*, 10.1007/s00704-
671 012-0787-7, 2012.
- 672 Björklund, J., Gunnarson, B. E., Seftigen, K., Esper, J., and Linderholm, H. W.: Blue intensity and
673 density from northern Fennoscandian tree rings, exploring the potential to improve summer

674 temperature reconstructions with earlywood information, *Climate of the Past*, 10, 877-885,
675 10.5194/cp-10-877-2014, 2014.

676 Briffa, K. R., Jones, P. D., Bartholin, T. S., Eckstein, D., Schweingruber, F. H., Karlén, W.,
677 Zetterberg, P., and Eronen, M.: Fennoscandian summers from ad 500: temperature changes on short
678 and long timescales, *Climate Dynamics*, 7, 111-119, 10.1007/bf00211153, 1992.

679 Briffa, K. R., and Melvin, T. M.: A Closer Look at Regional Curve Standardization of Tree-Ring
680 Records: Justification of the Need, a Warning of Some Pitfalls, and Suggested Improvements in Its
681 Application, in: *Dendroclimatology: Progress and Prospects*, edited by: Hughes, M. K., Swetnam, T.
682 W., and Diaz, H. F., Springer Netherlands, Dordrecht, 113-145, 2011.

683 Carley, E. I., and Gabriele, C. H.: The global precipitation response to volcanic eruptions in the
684 CMIP5 models, *Environmental Research Letters*, 9, 104012, 2014.

685 Coats, S., Cook, B. I., Smerdon, J. E., and Seager, R.: North American Pancontinental Droughts in
686 Model Simulations of the Last Millennium*, *Journal of Climate*, 28, 2025-2043, 10.1175/jcli-d-14-
687 00634.1, 2015.

688 Cook, E. R., Briffa, K. R., Meko, D., Graybill, D. A., and Funkhouser, G.: The 'segment length curse'
689 in long tree-ring chronology development for palaeoclimatic studies, *The Holocene*, 5, 229-237, 1995.

690 Cook, E. R., Meko, D. M., Stahle, D. W., and Cleaveland, M. K.: Drought Reconstructions for the
691 Continental United States, *Journal of Climate*, 12, 1145-1162, 1999.

692 Cook, E. R., and Krusic, P. J.: Arstan, version 2005, Tree-ring labora- tory, Lamont-Doherty Earth
693 Obs., Palisades, N. Y. (Available at <http://www.ldeo.columbia.edu/trl>), 2005.

694 Cook, E. R., Seager, R., Kushnir, Y., Briffa, K. R., Büntgen, U., Frank, D., Krusic, P. J., Tegel, W.,
695 van der Schrier, G., Andreu-Hayles, L., Baillie, M., Baittinger, C., Bleicher, N., Bonde, N., Brown, D.,
696 Carrer, M., Cooper, R., Čufar, K., Dittmar, C., Esper, J., Griggs, C., Gunnarson, B., Günther, B.,
697 Gutierrez, E., Haneca, K., Helama, S., Herzig, F., Heussner, K.-U., Hofmann, J., Janda, P., Kontic, R.,
698 Köse, N., Kyncl, T., Levanič, T., Linderholm, H., Manning, S., Melvin, T. M., Miles, D., Neuwirth,
699 B., Nicolussi, K., Nola, P., Panayotov, M., Popa, I., Rothe, A., Seftigen, K., Seim, A., Svarva, H.,
700 Svoboda, M., Thun, T., Timonen, M., Touchan, R., Trotsiuk, V., Trouet, V., Walder, F., Ważny, T.,
701 Wilson, R., and Zang, C.: Old World megadroughts and pluvials during the Common Era, *Science*
702 *Advances*, 1, 10.1126/sciadv.1500561, 2015.

703 Crowley, T. J., and Unterman, M. B.: Technical details concerning development of a 1200 yr proxy
704 index for global volcanism, *Earth Syst. Sci. Data*, 5, 187-197, 10.5194/essd-5-187-2013, 2013.

705 D'Arrigo, R., Wilson, R., and Anchukaitis, K. J.: Volcanic cooling signal in tree ring temperature
706 records for the past millennium, *Journal of Geophysical Research: Atmospheres*, 118, 9000-9010,
707 10.1002/jgrd.50692, 2013.

708 Drobyshev, I., Niklasson, M., Linderholm, H. W., Seftigen, K., Hickler, T., and Eggertsson, O.:
709 Reconstruction of a regional drought index in southern Sweden since AD 1750, *The Holocene*, 21,
710 667-679, 10.1177/0959683610391312, 2011.

711 Dufresne, J. L., Foujols, M. A., Denvil, S., Caubel, A., Marti, O., Aumont, O., Balkanski, Y., Bekki,
712 S., Bellenger, H., Benshila, R., Bony, S., Bopp, L., Braconnot, P., Brockmann, P., Cadule, P., Cheruy,
713 F., Codron, F., Cozic, A., Cugnet, D., de Noblet, N., Duvel, J. P., Ethé, C., Fairhead, L., Fichefet, T.,
714 Flavoni, S., Friedlingstein, P., Grandpeix, J. Y., Guez, L., Guilyardi, E., Hauglustaine, D., Hourdin, F.,
715 Idelkadi, A., Ghattas, J., Joussaume, S., Kageyama, M., Krinner, G., Labetoulle, S., Lahellec, A.,
716 Lefebvre, M. P., Lefevre, F., Levy, C., Li, Z. X., Lloyd, J., Lott, F., Madec, G., Mancip, M.,
717 Marchand, M., Masson, S., Meurdesoif, Y., Mignot, J., Musat, I., Parouty, S., Polcher, J., Rio, C.,
718 Schulz, M., Swingedouw, D., Szopa, S., Talandier, C., Terray, P., Viovy, N., and Vuichard, N.:
719 Climate change projections using the IPSL-CM5 Earth System Model: from CMIP3 to CMIP5,
720 *Climate Dynamics*, 40, 2123-2165, 10.1007/s00382-012-1636-1, 2013.

721 Esper, J., Frank, D. C., Timonen, M., Zorita, E., Wilson, R. J. S., Luterbacher, J., Holzammer, S.,
722 Fischer, N., Wagner, S., Nievergelt, D., Verstege, A., and Buntgen, U.: Orbital forcing of tree-ring
723 data, *Nature Clim. Change*, 2, 862-866, 2012.

724 Esper, J., Schneider, L., Smerdon, J. E., Schöne, B. R., and Büntgen, U.: Signals and memory in tree-
725 ring width and density data, *Dendrochronologia*, 35, 62-70,
726 <http://dx.doi.org/10.1016/j.dendro.2015.07.001>, 2015.

727 Feng, S., Hu, Q., and Oglesby, R. J.: Influence of Atlantic sea surface temperatures on persistent
728 drought in North America, *Climate Dynamics*, 37, 569-586, 10.1007/s00382-010-0835-x, 2011.

729 Fischer, E. M., Luterbacher, J., Zorita, E., Tett, S. F. B., Casty, C., and Wanner, H.: European climate
730 response to tropical volcanic eruptions over the last half millennium, *Geophysical Research Letters*,
731 34, n/a-n/a, 10.1029/2006GL027992, 2007.

732 Frank, D. C., Esper, J., and Cook, E. R.: On variance adjustments in tree-ring chronology
733 development, *Tree rings in archaeology, climatology and ecology*, TRACE, 4, 56-66, 2006.

734 Franke, J., Frank, D., Raible, C. C., Esper, J., and Bronnimann, S.: Spectral biases in tree-ring climate
735 proxies, *Nature Clim. Change*, 3, 360-364, 2013.

736 Gao, C., Robock, A., and Ammann, C.: Volcanic forcing of climate over the past 1500 years: An
737 improved ice core-based index for climate models, *Journal of Geophysical Research: Atmospheres*,
738 113, n/a-n/a, 10.1029/2008JD010239, 2008.

739 Gentine, P., Holtslag, A. A. M., D'Andrea, F., and Ek, M.: Surface and Atmospheric Controls on the
740 Onset of Moist Convection over Land, *Journal of Hydrometeorology*, 14, 1443-1462, 10.1175/jhm-d-
741 12-0137.1, 2013.

742 Gleckler, P. J., Wigley, T. M. L., Santer, B. D., Gregory, J. M., AchutaRao, K., and Taylor, K. E.:
743 Volcanoes and climate: Krakatoa's signature persists in the ocean, *Nature*, 439, 675-675, 2006.

744 Grinsted, A., Moore, J. C., and Jevrejeva, S.: Application of the cross wavelet transform and wavelet
745 coherence to geophysical time series, *Nonlin. Processes Geophys.*, 11, 561-566, 10.5194/npg-11-561-
746 2004, 2004.

747 Gunnarson, B. E., Linderholm, H. W., and Moberg, A.: Improving a tree-ring reconstruction from
748 west-central Scandinavia: 900 years of warm-season temperatures, *Climate Dynamics*, 36, 97-108,
749 10.1007/s00382-010-0783-5, 2011.

750 Haarsma, R. J., Selden, F., Hurk, B. v., Hazeleger, W., and Wang, X.: Drier Mediterranean soils due to
751 greenhouse warming bring easterly winds over summertime central Europe, *Geophysical Research*
752 *Letters*, 36, n/a-n/a, 10.1029/2008GL036617, 2009.

753 Harris, I., Jones, P. D., Osborn, T. J., and Lister, D. H.: Updated high-resolution grids of monthly
754 climatic observations – the CRU TS3.10 Dataset, *International Journal of Climatology*, 34, 623-642,
755 10.1002/joc.3711, 2014.

756 Haurwitz, M. W., and Brier, G. W.: A Critique of the Superposed Epoch Analysis Method: Its
757 Application to Solar–Weather Relations, *Monthly Weather Review*, 109, 2074-2079, 10.1175/1520-
758 0493(1981)109<2074:acotse>2.0.co;2, 1981.

759 Hegerl, G. C., Black, E., Allan, R. P., Ingram, W. J., Polson, D., Trenberth, K. E., Chadwick, R. S.,
760 Arkin, P. A., Sarojini, B. B., Becker, A., Dai, A., Durack, P. J., Easterling, D., Fowler, H. J., Kendon,
761 E. J., Huffman, G. J., Liu, C., Marsh, R., New, M., Osborn, T. J., Skliris, N., Stott, P. A., Vidale, P.-L.,
762 Wijffels, S. E., Wilcox, L. J., Willett, K. M., and Zhang, X.: Challenges in Quantifying Changes in the
763 Global Water Cycle, *Bulletin of the American Meteorological Society*, 96, 1097-1115, 10.1175/bams-
764 d-13-00212.1, 2015.

765 Helama, S., and Lindholm, M.: Droughts and rainfall in south eastern Finland since AD 874, inferred
766 from Scots pine tree-rings, *Boreal Environ Res*, 8, 171-183, 2003.

767 Helama, S., Merilainen, J., and Tuomenvirta, H.: Multicentennial megadrought in northern Europe
768 coincided with a global El Nino-Southern Oscillation drought pattern during the Medieval Climate
769 Anomaly, *Geology*, 37, 175-178, 10.1130/g25329a.1, 2009.

770 Held, I. M., and Soden, B. J.: Robust Responses of the Hydrological Cycle to Global Warming,
771 *Journal of Climate*, 19, 5686-5699, 10.1175/jcli3990.1, 2006.

772 Iles, C. E., Hegerl, G. C., Schurer, A. P., and Zhang, X.: The effect of volcanic eruptions on global
773 precipitation, *Journal of Geophysical Research: Atmospheres*, 118, 8770-8786, 10.1002/jgrd.50678,
774 2013.

775 Iles, C. E., and Hegerl, G. C.: Systematic change in global patterns of streamflow following volcanic
776 eruptions, *Nature Geoscience*, 8, 838-842, 10.1038/ngeo2545, 2015.

777 Jones, P. D., Osborn, T. J., and Briffa, K. R.: Estimating Sampling Errors in Large-Scale Temperature
778 Averages, *Journal of Climate*, 10, 2548-2568, 10.1175/1520-0442(1997)010<2548:eseils>2.0.co;2,
779 1997.

780 Jones, P. D., and Lister, D. H.: The influence of the circulation on surface temperature and
781 precipitation patterns over Europe, *Clim. Past*, 5, 259-267, 10.5194/cp-5-259-2009, 2009.

782 Jones, P. D., Melvin, T. M., Harpham, C., Grudd, H., and Helama, S.: Cool North European summers
783 and possible links to explosive volcanic eruptions, *Journal of Geophysical Research: Atmospheres*,
784 118, 6259-6265, 10.1002/jgrd.50513, 2013.

785 Jönsson, K., and Nilsson, C.: Scots Pine (*pinus sylvestris*L.) on Shingle Fields: A Dendrochronologic
786 Reconstruction of Early Summer Precipitation in Mideast Sweden, *Journal of Climate*, 22, 4710-4722,
787 10.1175/2009jcli2401.1, 2009.

788 Jungclaus, J. H., Lohmann, K., and Zanchettin, D.: Enhanced 20th-century heat transfer to the Arctic
789 simulated in the context of climate variations over the last millennium, *Clim. Past*, 10, 2201-2213,
790 10.5194/cp-10-2201-2014, 2014.

791 Kavvada, A., Ruiz-Barradas, A., and Nigam, S.: AMO's structure and climate footprint in
792 observations and IPCC AR5 climate simulations, *Climate Dynamics*, 41, 1345-1364, 10.1007/s00382-
793 013-1712-1, 2013.

794 Landrum, L., Otto-Bliesner, B. L., Wahl, E. R., Conley, A., Lawrence, P. J., Rosenbloom, N., and
795 Teng, H.: Last Millennium Climate and Its Variability in CCSM4, *Journal of Climate*, 26, 1085-1111,
796 10.1175/JCLI-D-11-00326.1, 2012.

797 Lehner, F., Joos, F., Raible, C. C., Mignot, J., Born, A., Keller, K. M., and Stocker, T. F.: Climate and
798 carbon cycle dynamics in a CESM simulation from 850 to 2100 CE, *Earth Syst. Dynam.*, 6, 411-434,
799 10.5194/esd-6-411-2015, 2015.

800 Linderholm, H., and Molin, T.: Early nineteenth century drought in east central Sweden inferred from
801 dendrochronological and historical archives, *Climate Research*, 29, 63-72, 2005.

802 Linderholm, H. W., Niklasson, M., and Molin, T.: Summer Moisture Variability in East Central
803 Sweden Since the Mid-Eighteenth Century Recorded in Tree Rings, *Geografiska Annaler: Series A,*
804 *Physical Geography*, 86, 277-287, 10.1111/j.0435-3676.2004.00231.x, 2004.

805 Linderholm, H. W., Björklund, J., Seftigen, K., Gunnarson, B. E., Grudd, H., Jeong, J.-H., Drobyshv,
806 I., and Liu, Y.: Dendroclimatology in Fennoscandia – from past accomplishments to future potential,
807 *Climate of the Past*, 6, 93-114, 2010.

808 Linderholm, H. W., Björklund, J., Seftigen, K., Gunnarson, B. E., and Fuentes, M.: Fennoscandia
809 revisited: a spatially improved tree-ring reconstruction of summer temperatures for the last 900 years,
810 *Climate Dynamics*, 45, 933-947, 10.1007/s00382-014-2328-9, 2014.

811 Madden, R. A., and Williams, J.: The Correlation between Temperature and Precipitation in the
812 United States and Europe, *Monthly Weather Review*, 106, 142-147, 10.1175/1520-
813 0493(1978)106<0142:tcbtap>2.0.co;2, 1978.

814 McCarroll, D., Loader, N. J., Jalkanen, R., Gagen, M. H., Grudd, H., Gunnarson, B. E., Kirchhefer, A.,
815 Friedrich, M., Linderholm, H. W., Lindholm, M., Boettger, T., Los, S. O., Remmele, S., Kononov,
816 Y. M., Yamazaki, Y. H., Young, G. H., and Zorita, E.: A 1200-year multiproxy record of tree growth
817 and summer temperature at the northern pine forest limit of Europe, *The Holocene*, 23, 471-484,
818 10.1177/0959683612467483, 2013.

819 Melvin, T. M., and Briffa, K. R.: A “signal-free” approach to dendroclimatic standardisation,
820 *Dendrochronologia*, 26, 71-86, 10.1016/j.dendro.2007.12.001, 2008.

821 National Research Council: *Surface Temperature Reconstructions for the Last 2,000 Years*, The
822 National Academies Press, Washington, DC978-0-309-10225-4, 160, 2006.

823 Oglesby, R., Feng, S., Hu, Q., and Rowe, C.: The role of the Atlantic Multidecadal Oscillation on
824 medieval drought in North America: Synthesizing results from proxy data and climate models, *Global*
825 *Planet Change*, 84–85, 56-65, <http://dx.doi.org/10.1016/j.gloplacha.2011.07.005>, 2012.

826 Osborn, T. J.: Simulating the winter North Atlantic Oscillation: the roles of internal variability and
827 greenhouse gas forcing, *Climate Dynamics*, 22, 605-623, 10.1007/s00382-004-0405-1, 2004.

828 Otto-Bliesner, B. L., Brady, E. C., Fasullo, J., Jahn, A., Landrum, L., Stevenson, S., Rosenbloom, N.,
829 Mai, A., and Strand, G.: Climate Variability and Change since 850 CE: An Ensemble Approach with
830 the Community Earth System Model, *Bulletin of the American Meteorological Society*, 97, 735-754,
831 10.1175/bams-d-14-00233.1, 2016.

832 Sarojini, B. B., Stott, P. A., and Black, E.: Detection and attribution of human influence on regional
833 precipitation, *Nature Clim. Change*, 6, 669-675, 10.1038/nclimate2976, 2016.

834 Schmidt, G. A., Jungclaus, J. H., Ammann, C. M., Bard, E., Braconnot, P., Crowley, T. J., Delaygue,
835 G., Joos, F., Krivova, N. A., Muscheler, R., Otto-Bliesner, B. L., Pongratz, J., Shindell, D. T., Solanki,
836 S. K., Steinhilber, F., and Vieira, L. E. A.: Climate forcing reconstructions for use in PMIP

837 simulations of the last millennium (v1.0), *Geosci. Model Dev.*, 4, 33-45, 10.5194/gmd-4-33-2011,
838 2011.

839 Seftigen, K., Linderholm, H. W., Drobyshev, I., and Niklasson, M.: Reconstructed drought variability
840 in southeastern Sweden since the 1650s, *International Journal of Climatology*, 33, 2449-2458,
841 10.1002/joc.3592, 2013.

842 Seftigen, K., Björklund, J., Cook, E. R., and Linderholm, H. W.: A tree-ring field reconstruction of
843 Fennoscandian summer hydroclimate variability for the last millennium, *Climate Dynamics*, 44, 3141-
844 3154, 10.1007/s00382-014-2191-8, 2014.

845 Seftigen, K., Cook, E., Linderholm, H., Fuentes, M., and Björklund, J.: The Potential of Deriving
846 Tree-Ring-Based Field Reconstructions of Droughts and Pluvials over Fennoscandia, *Journal of*
847 *Climate*, 28, 3453-3471, 10.1175/JCLI-D-13-00734.s1, 2015.

848 Seneviratne, S. I., Corti, T., Davin, E. L., Hirschi, M., Jaeger, E. B., Lehner, I., Orlowsky, B., and
849 Teuling, A. J.: Investigating soil moisture–climate interactions in a changing climate: A review, *Earth-*
850 *Science Reviews*, 99, 125-161, <http://dx.doi.org/10.1016/j.earscirev.2010.02.004>, 2010.

851 Shindell, D. T., Schmidt, G. A., Mann, M. E., and Faluvegi, G.: Dynamic winter climate response to
852 large tropical volcanic eruptions since 1600, *Journal of Geophysical Research: Atmospheres*, 109, n/a-
853 n/a, 10.1029/2003JD004151, 2004.

854 Sigl, M., Winstrup, M., McConnell, J. R., Welten, K. C., Plunkett, G., Ludlow, F., Buntgen, U.,
855 Caffee, M., Chellman, N., Dahl-Jensen, D., Fischer, H., Kipfstuhl, S., Kostick, C., Maselli, O. J.,
856 Mekhaldi, F., Mulvaney, R., Muscheler, R., Pasteris, D. R., Pilcher, J. R., Salzer, M., Schupbach, S.,
857 Steffensen, J. P., Vinther, B. M., and Woodruff, T. E.: Timing and climate forcing of volcanic
858 eruptions for the past 2,500 years, *Nature*, 523, 543-549, 2015.

859 Taylor, K. E., Stouffer, R. J., and Meehl, G. A.: An Overview of CMIP5 and the Experiment Design,
860 *Bulletin of the American Meteorological Society*, 93, 485-498, 10.1175/bams-d-11-00094.1, 2012.

861 Thiéblemont, R., Matthes, K., Omrani, N.-E., Kodera, K., and Hansen, F.: Solar forcing synchronizes
862 decadal North Atlantic climate variability, *Nature communications*, 6, 8268, 2015.

863 Thomson, D. J.: Spectrum estimation and harmonic analysis, *Proceedings of the IEEE*, 70, 1055-1096,
864 10.1109/PROC.1982.12433, 1982.

865 Thornthwaite, C. W.: An Approach Toward a Rational Classification of Climate, *Soil Science*, 66, 77,
866 1948.

867 Tolwinski-Ward, S., Evans, M. N., Hughes, M. K., and Anchukaitis, K. J.: An efficient forward model
868 of the climate controls on interannual variation in tree-ring width, *Climate Dynamics*, 36, 2419-2439,
869 10.1007/s00382-010-0945-5, 2011.

870 Trenberth, K. E.: Changes in precipitation with climate change, *Climate Research*, 47, 123-138,
871 10.3354/cr00953, 2011.

872 van Oldenborgh, G. J., and Van Ulden, A. A. D.: On the relationship between global warming, local
873 warming in the Netherlands and changes in circulation in the 20th century, *International Journal of*
874 *Climatology*, 23, 1711-1724, 10.1002/joc.966, 2003.

875 Vicente-Serrano, S. M., Beguería, S., and López-Moreno, J. I.: A Multiscalar Drought Index Sensitive
876 to Global Warming: The Standardized Precipitation Evapotranspiration Index, *Journal of Climate*, 23,
877 1696-1718, 10.1175/2009jcli2909.1, 2010.

878 Vicente-Serrano, S. M., Gouveia, C., Camarero, J. J., Beguería, S., Trigo, R., López-Moreno, J. I.,
879 Azorín-Molina, C., Pasho, E., Lorenzo-Lacruz, J., Revuelto, J., Morán-Tejeda, E., and Sanchez-
880 Lorenzo, A.: Response of vegetation to drought time-scales across global land biomes, *Proceedings of*
881 *the National Academy of Sciences*, 110, 52-57, 10.1073/pnas.1207068110, 2013.

882 Watanabe, S., Hajima, T., Sudo, K., Nagashima, T., Takemura, T., Okajima, H., Nozawa, T., Kawase,
883 H., Abe, M., Yokohata, T., Ise, T., Sato, H., Kato, E., Takata, K., Emori, S., and Kawamiya, M.:
884 MIROC-ESM 2010: model description and basic results of CMIP5-20c3m experiments, *Geosci.*
885 *Model Dev.*, 4, 845-872, 10.5194/gmd-4-845-2011, 2011.

886 Wigley, T. M. L., Briffa, K. R., and Jones, P. D.: On the Average Value of Correlated Time Series,
887 with Applications in Dendroclimatology and Hydrometeorology, *Journal of Climate and Applied*
888 *Meteorology*, 23, 201-213, 10.1175/1520-0450(1984)023<0201:otavoc>2.0.co;2, 1984.

889 Wilson, R., Miles, D., Loader, N. J., Melvin, T., Cunningham, L., Cooper, R., and Briffa, K.: A
890 millennial long March–July precipitation reconstruction for southern-central England, *Climate*
891 *Dynamics*, 10.1007/s00382-012-1318-z, 2012.

892 Wilson, R., Anchukaitis, K., Briffa, K. R., Büntgen, U., Cook, E., D'Arrigo, R., Davi, N., Esper, J.,
893 Frank, D., Gunnarson, B., Hegerl, G., Helama, S., Klesse, S., Krusic, P. J., Linderholm, H. W.,
894 Myglan, V., Osborn, T. J., Rydval, M., Schneider, L., Schurer, A., Wiles, G., Zhang, P., and Zorita, E.:
895 Last millennium northern hemisphere summer temperatures from tree rings: Part I: The long term
896 context, *Quaternary Science Reviews*, 134, 1-18, 10.1016/j.quascirev.2015.12.005, 2016.
897 Wu, P., Christidis, N., and Stott, P.: Anthropogenic impact on Earth's hydrological cycle, *Nature*
898 *Clim. Change*, 3, 807-810, 2013.
899 Wu, T., Song, L., Li, W., Wang, Z., Zhang, H., Xin, X., Zhang, Y., Zhang, L., Li, J., Wu, F., Liu, Y.,
900 Zhang, F., Shi, X., Chu, M., Zhang, J., Fang, Y., Wang, F., Lu, Y., Liu, X., Wei, M., Liu, Q., Zhou,
901 W., Dong, M., Zhao, Q., Ji, J., Li, L., and Zhou, M.: An overview of BCC climate system model
902 development and application for climate change studies, *Journal of Meteorological Research*, 28, 34-
903 56, 10.1007/s13351-014-3041-7, 2014.
904 Zhang, H., Yuan, N., Esper, J., Werner, J. P., Xoplaki, E., Büntgen, U., Treydte, K., and Luterbacher,
905 J.: Modified climate with long term memory in tree ring proxies, *Environmental Research Letters*, 10,
906 084020, 10.1088/1748-9326/10/8/084020, 2015.
907 Zhang, X., Zwiers, F. W., Hegerl, G. C., Lambert, F. H., Gillett, N. P., Solomon, S., Stott, P. A., and
908 Nozawa, T.: Detection of human influence on twentieth-century precipitation trends, *Nature*, 448, 461-
909 465, 2007.

910

911

912

913

914

915

916

917

918

919

920

921

922

923

924

925 **Tables and figures**

926 **Table I.** CMIP5/PMIP3 model description.

Model Name	Resolution [Atmosphere]	Resolution [Ocean]	Reference
CCSM4	192 x 288	384 x 320	Landrum et al. (2012)
CESM1	96 x 144	384 x 320	Lehner et al. (2015)
IPSL-CM5A-LR	96 x 96	149 x 182	Dufresne et al. (2013)
MIROC-ESM	64 x 128	192 x 256	Watanabe et al. (2011)
MPI-ESM-P	96 x 192	220 x 256	Jungclaus et al. (2014)
BCC-CSM1-1	64 x 128	232 x 360	Wu et al. (2014)

927 **Table II:** Tree-ring network description.

Site	Coord.	Time coverage	Standardization method	MSL ³	Source
Eastern Finland	61.87N, 28.90E	535 -2002 CE	RCS ¹	147 yrs	Helama et al. (2009) Online resource: http://lustiag.pp.fi/Saima/dendrotieto.htm Date access: January 2013
Gotland Sweden	57.49N, 18.41E	1127-2011 CE	RCS	130 yrs	Investigator: Schweingruber, F.H. Online resource: https://www.ncdc.noaa.gov/paleo/study/4427 Date access: January 2013 Updated in Seftigen et al. (2015) *
Jondalen Norway	59.71N, 9.53E	1185 -2011 CE	RCS	165 yrs	Investigator: Briffa, K. Online resource: https://www.ncdc.noaa.gov/paleo/study/2826 Date access: January 2013 Updated in Seftigen et al. (2015) *
Baljåsen Sweden	59.04N, 12.27E	1686-2002 CE	SF2 ²	174 yrs	Seftigen et al. (2015)*
Björbo Sweden	60.27N, 14.44E	1450-2011 CE	SF	177 yrs	Investigator: Axelson, T. Online resource: https://www.ncdc.noaa.gov/paleo/study/2667 Date access: January 2013
Ekhultebergen Sweden	57.45N, 13.50E	1705-2008 CE	SF1	215 yrs	Seftigen et al. (2015) *
Fårhagsberget Sweden	58.08N, 16.14E	1621-2011 CE	SF1	262 yrs	Seftigen et al. (2015) *
Helvetets håla Sweden	57.14N, 16.14E	1691-2011 CE	SF1	255 yrs	Seftigen et al. (2015) *
Halle-Vagnaren Sweden	57.17N, 15.17E	1718-2009 CE	SF3	186 yrs	Seftigen et al. (2015) *
Hornslandet Sweden	59.01N, 11.08E	1590-2011 CE	SF1	270 yrs	Seftigen et al. (2015) *
Korphålorna Sweden	61.43N, 17.00E	1790-2011 CE	SF1	199 yrs	Seftigen et al. (2015) *
Myrkaby Sweden	57.45N, 15.23E	1669-2011 CE	SF2	294 yrs	Seftigen et al. (2015) *
Nämndö Sweden	59.52N, 16.56E	1582-1995 CE	SF1	123 yrs	Investigator: Larsson, L. Online resource: https://www.ncdc.noaa.gov/paleo/study/3869 Date access: January 2013
Valekleven-Ombo Sweden	59.11N, 18.41E	1578-2011 CE	SF1	225 yrs	Seftigen et al. (2015) *
Putbergen Sweden	58.37N, 14.32E	1734-2008 CE	SF1	188 yrs	Seftigen et al. (2015) *
Salboknös Sweden	59.11N, 16.55E	1486-2011 CE	SF2	357 yrs	Seftigen et al. (2015) *
Särö Sweden	61.92N, 11.93E	1712-2002 CE	SF3	176 yrs	Seftigen et al. (2015) *
Sisshammer Sweden	59.46N, 14.54E	1661-2003 CE	SF	74 yrs	Investigator: Andreason, T. Online resource: https://www.ncdc.noaa.gov/paleo/study/2663 Date access: January 2013
Skärmarbodabergen Sweden	57.51N, 11.93E	1600-2002 CE	SF3	160 yrs	Seftigen et al. (2015) *
Skitåsen Sweden	59.09N, 18.02E	1672-2011 CE	SF2	285 yrs	Seftigen et al. (2015) *
Skuleskogen Sweden	59.26N, 15.07E	1448-2011 CE	SF	181 yrs	Seftigen et al. (2015) *
Sörknatten Sweden	59.22N, 15.29E	1762-2009 CE	SF3	197 yrs	Seftigen et al. (2015) *
Tjurhults mosse Sweden	63.06N, 18.29E	1655-2011 CE	SF2	268 yrs	Seftigen et al. (2015) *
Tjusthult Sweden	58.55N, 12.27E	1681-2011 CE	SF1	221 yrs	Seftigen et al. (2015) *
Tyresta Sweden	59.52N, 14.71E	1609-2010 CE	SF1	198 yrs	Linderholm and Molin (2005) Updated in Seftigen et al. (2015) *

928 ¹RCS: Regional Curve Standardization;

929 ²SF: Signal-Free Standardization. The number after the abbreviation indicates the PCA cluster number (Fig. S2);

930 ³MSL: Mean Segment Length;

931 * Unprocessed tree-ring series are available as supplementary material.

932 **Table III.** Event years used in the Superposed Epoch Analysis (Fig. 4). The event lists are composed
 933 of the 20 strongest eruptions from each record.

Source	Event years (CE)
Gao et al. (2008) (sulfate aerosol > 15 Tg)	1167, 1176, 1195, 1227, 1258, 1284, 1328, 1452, 1459, 1584, 1600, 1641, 1719, 1783, 1809, 1815, 1831, 1835, 1991
Crowley and Unterman (2013) (AOD > 0.13)	1229, 1258, 1259, 1286, 1287, 1456, 1457, 1600, 1601, 1641, 1695, 1696, 1809, 1810, 1815, 1816, 1817, 1884, 1992
Sigl et al. (2015) (global forcing < 5.86 W/m ²)	1108, 1171, 1191, 1230, 1258, 1276, 1286, 1345, 1453, 1458, 1601, 1641, 1695, 1783, 1809, 1815, 1832, 1836, 1992

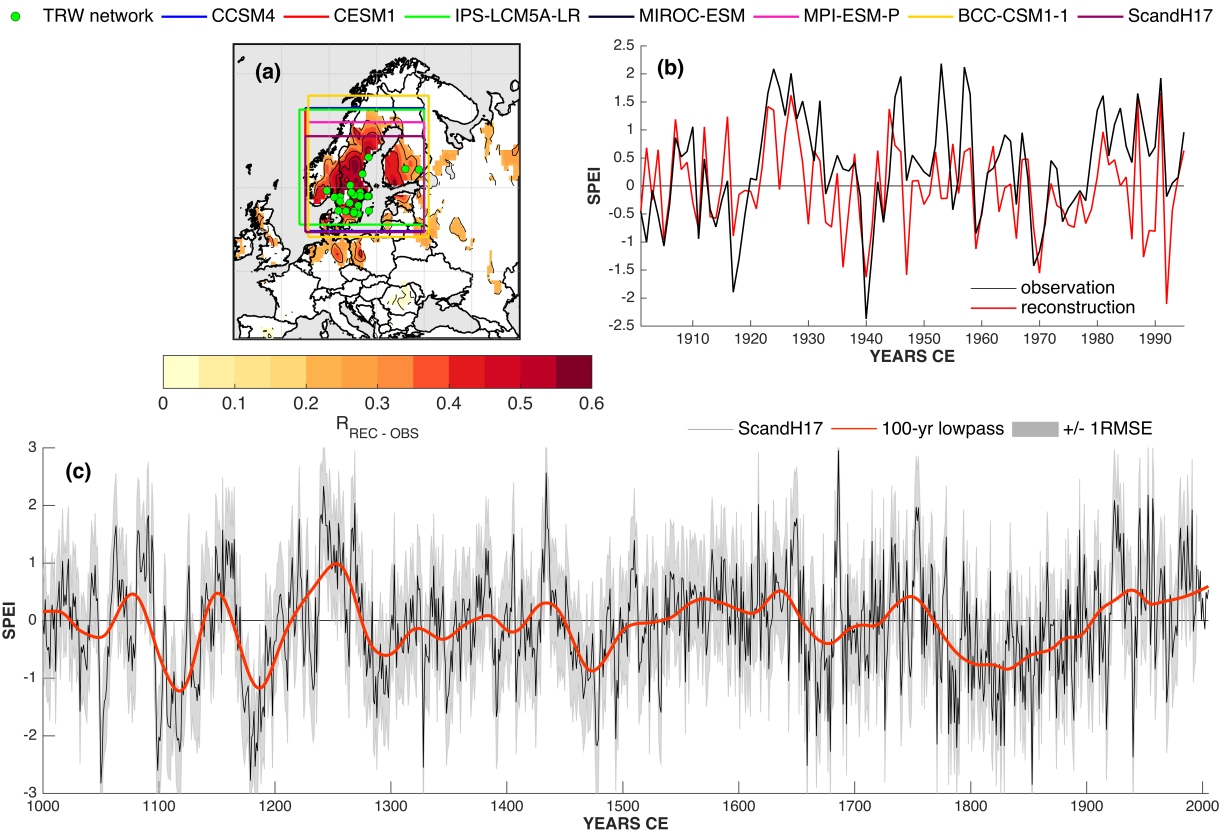


Figure 1: Average regional warm-season SPEI time series reconstructed from tree-rings. (a) Location of the tree-ring network used for regional reconstruction and the extent of the CMIP5/PMIP3 model precipitation and temperature grids used to derive regional SPEI estimates. Shaded contours display the correlation ($p < 0.1$) between the tree-ring reconstruction and fields of instrumental SPEI data over the 1901-1995 period; (b) average regional reconstructed and instrumental 20th century 2-month June SPEI; (c) average regional SPEI nested reconstruction, with the ± 1 RMSE of the regression equations outlined in grey shading. A smoothed version of the reconstruction using a 100-year loess smooth is shown in red. Reconstruction assessment metrics are provided in supplementary materials (Fig. S4).

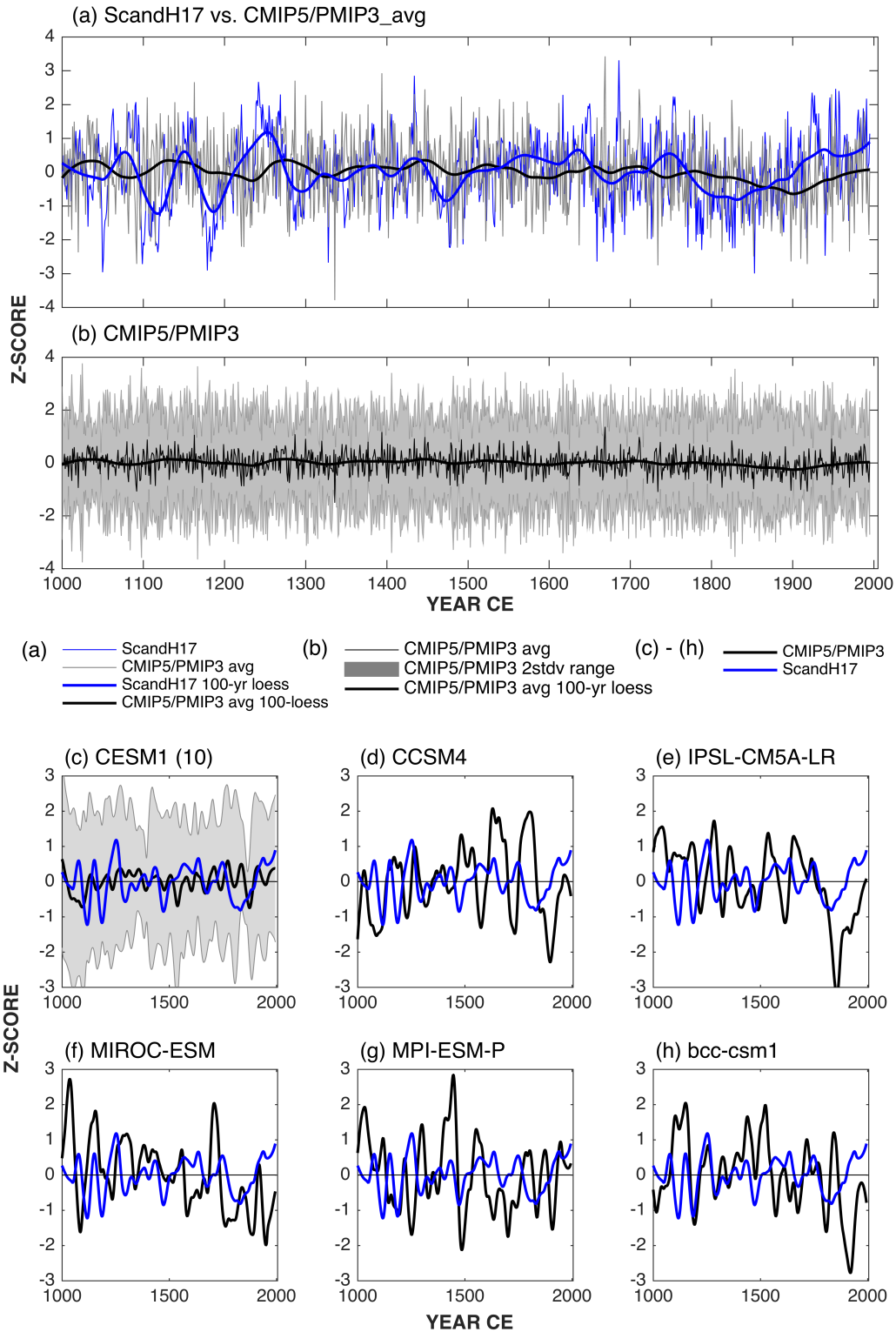


Figure 2: Comparison of reconstructed SPEI with forced model runs. (a) The reconstruction versus the mean of the six CMIP5/PMIP3 models transformed into standard normal deviates (z-scores) over the 1000-1995 CE period and smoothed with 100-year loess filter; (b) multimodel mean and the two standard deviation range (shading) of the six GCMs; (c) mean and two standard deviation (shading) of CESM1 ten smoothed and z-scored ensemble members (blue) together; (d) – (h) the

reconstruction (blue) versus individual model runs (black). All time series have been smoothed with 100-year loess filter and then z-scored over the 1000-1995 CE period.

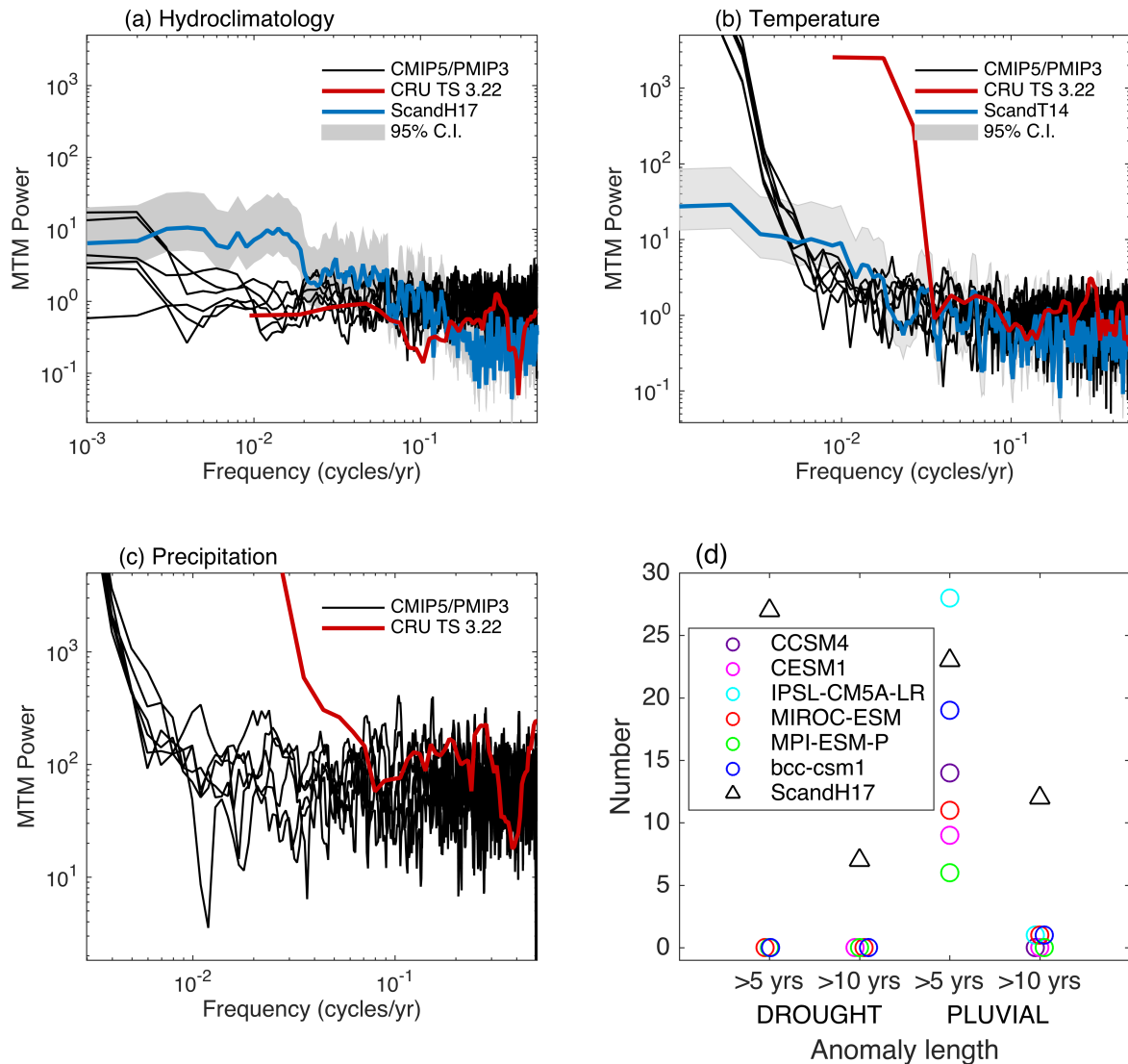


Figure 3: Spectral properties (multi-taper approach, 4 tapers) of (a) SPEI, (b) temperature and (c) precipitation over the common 1100-1995 period. For SPEI and temperature, the spectral properties of individual GCMs (r1i1p1 ensemble) are compared to those of the tree-ring ScandH17 and ScandT14 reconstructions and regionally averaged instrumental CRU TS 3.22 data. Shaded areas show the 95% confidence interval of the reconstruction spectra. (d) The number of droughts and pluvials in the reconstructed and simulated time series that are > 5 and >10 years in duration. Spectral properties of the individual models are provided in Fig. S7.

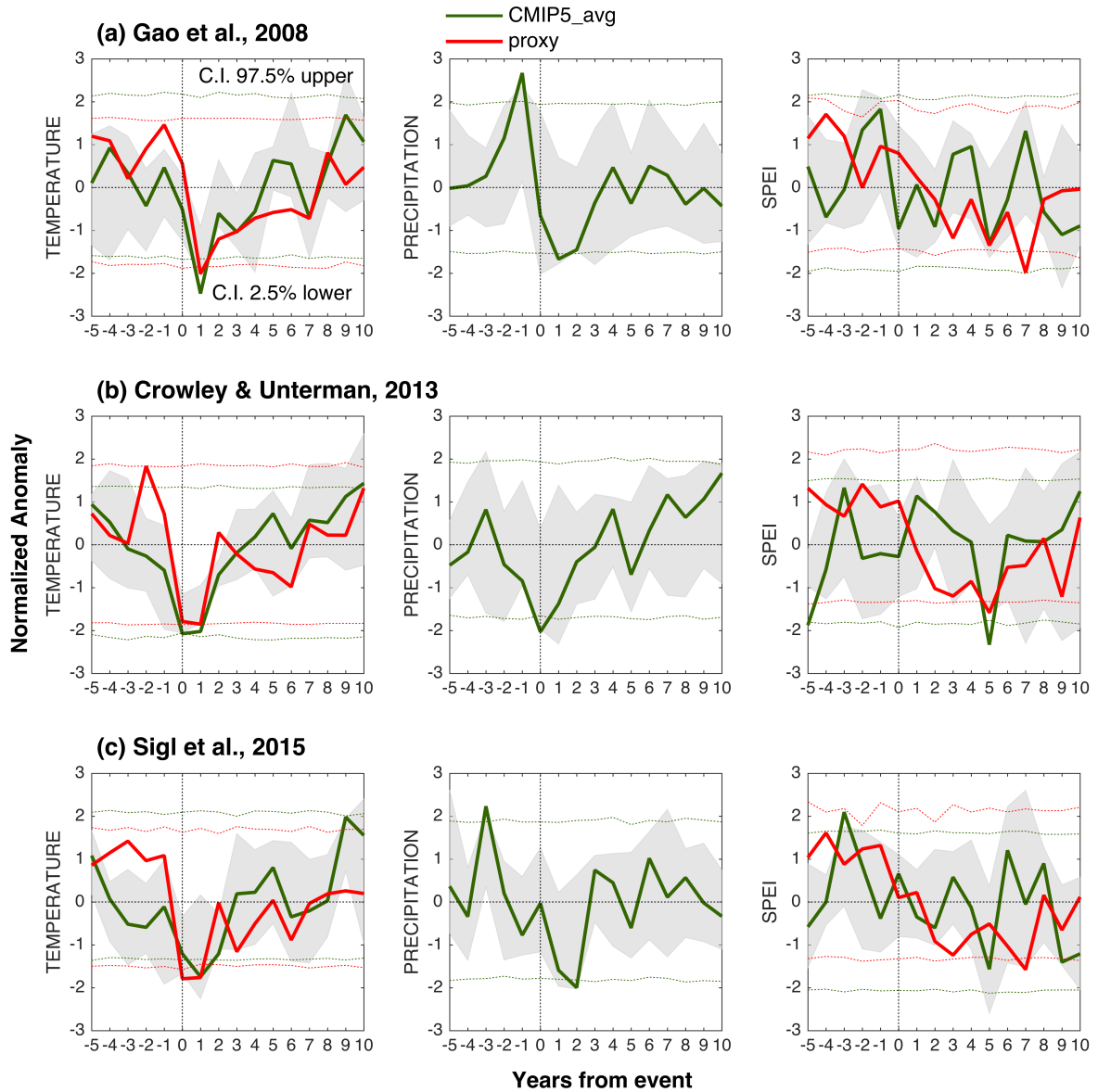


Figure 4: Modeled and reconstructed hydroclimate response to eruptions. Superposed epoch analysis using the 20 largest eruption years from the (a) Gao et al. (2008), (b) Crowley and Unterman (2013), and (c) Sigl et al. (2015). Table III lists the event years used in the analysis. Grey shading indicate the range of modeled hydroclimate response from the six GCMs. Confidence intervals (C.I.) are derived from bootstrap resampling ($N = 10\,000$).

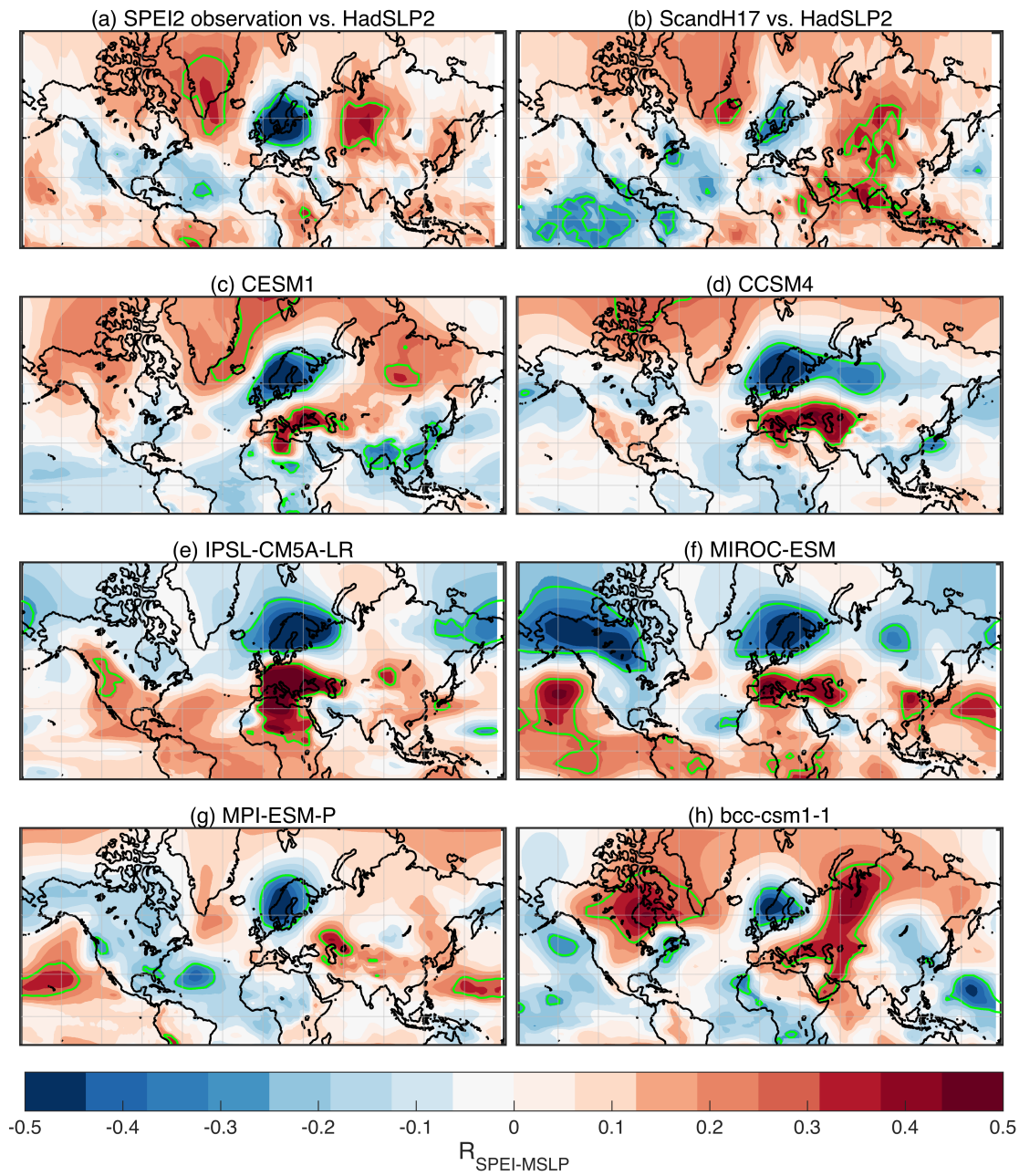


Figure 5: Spatial distribution of correlation coefficient of northern European warm season hydroclimate and mean sea level pressure (MSLP). Association between regional drought index and sea level pressure over the 1950-1995 period. (a) observational, (b) ScandH17, (c)-(g) model based results (including r1i1p1 ensemble only). Regions with significant ($p < 0.05$) correlations are outlined in green contours.

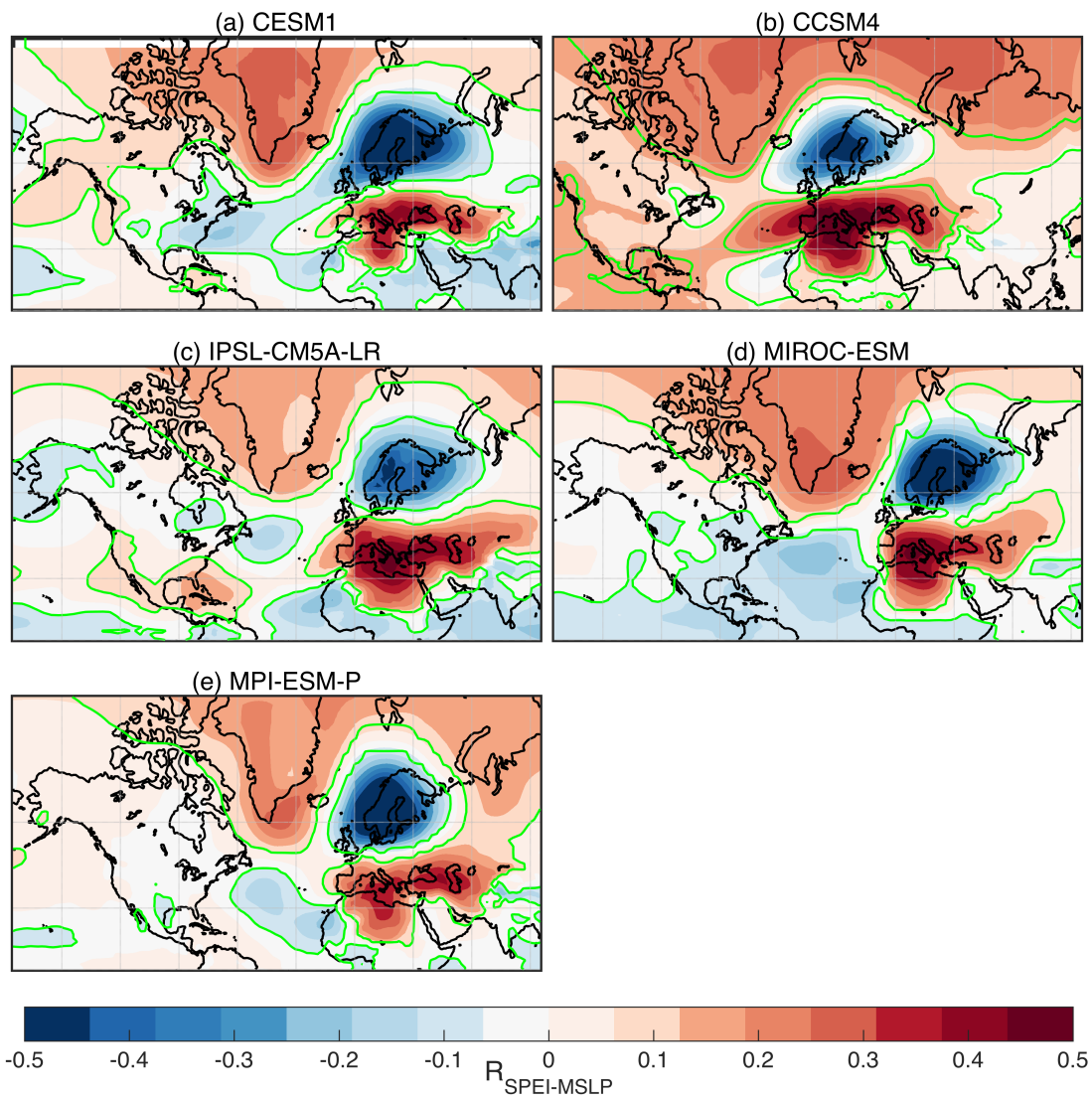


Figure 6: Spatial distribution of correlation coefficient of northern European warm season hydroclimate and mean sea level pressure (MSLP). Same as Fig. 5, but for the 850-1849 CE period.

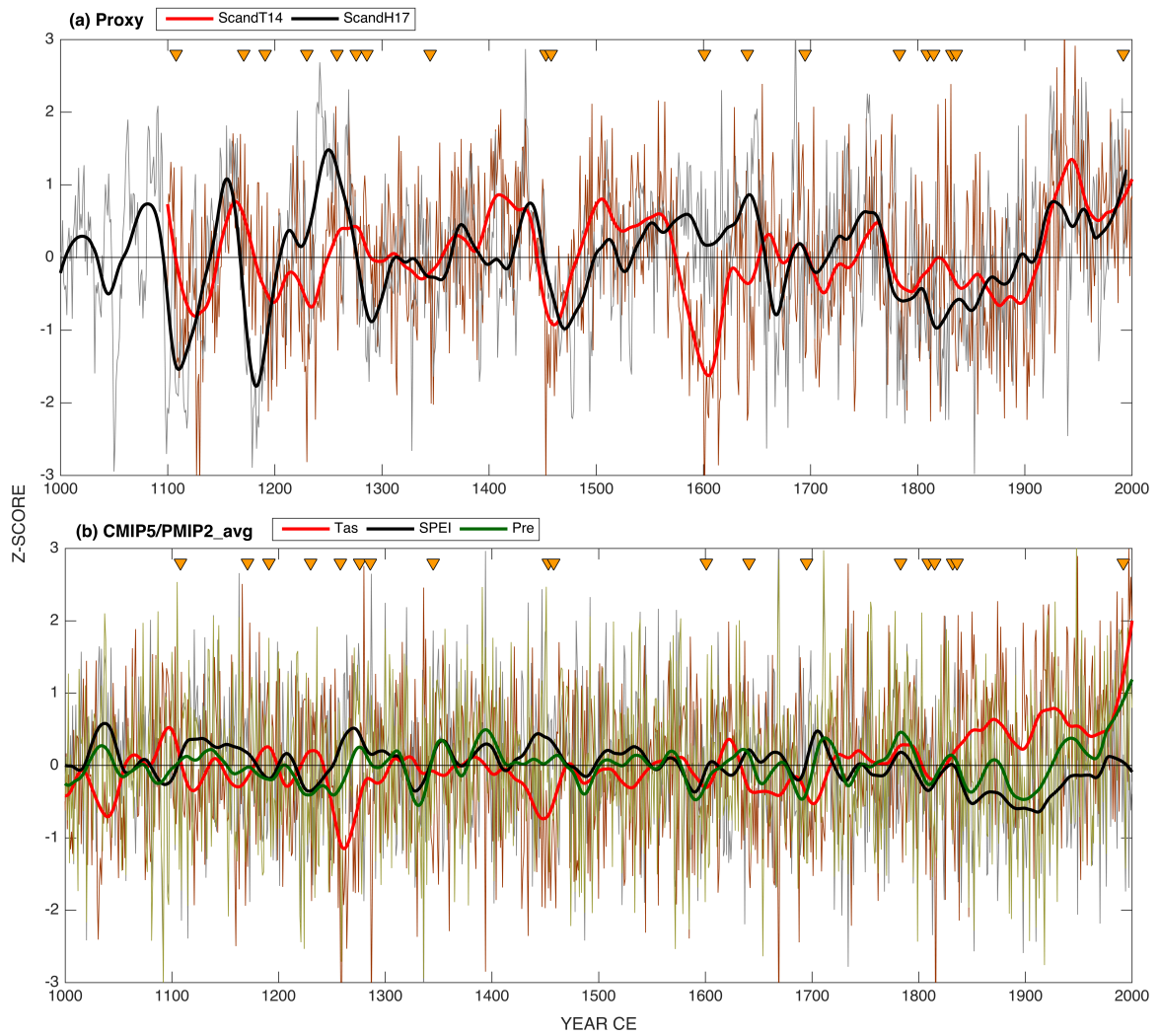


Figure 7: Time series of (a) ScandH17 and ScandT14, and (b) GCM (r1i1p1 ensemble) average temperature, precipitation and SPEI. Smoothed time-series using a 50-year loess filter are shown as thick lines. Individual model data are provided in supplementary material (Fig. S8). The years with volcanic eruptions from Table III are indicated by triangle glyphs.

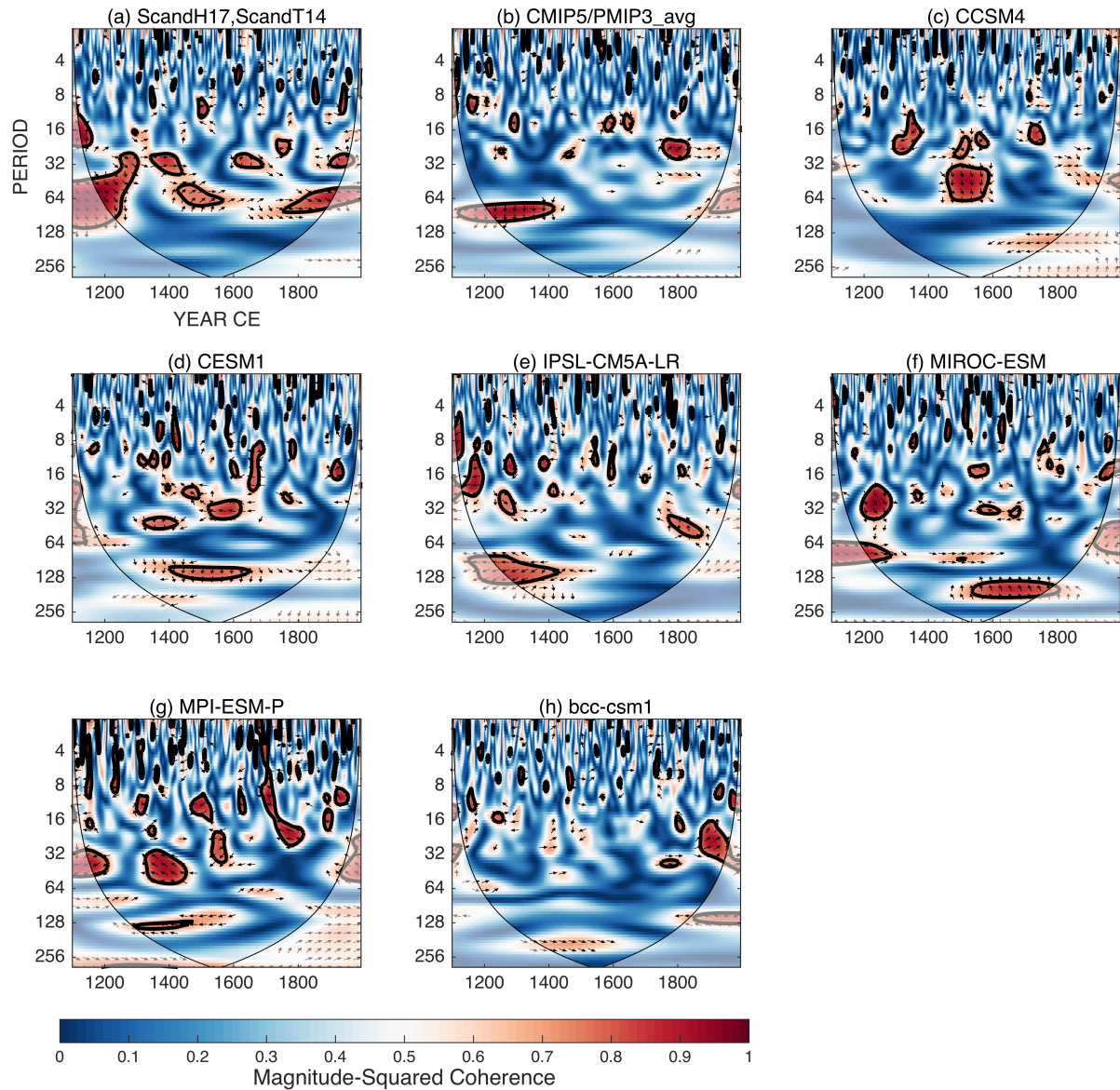


Figure 8: Squared wavelet coherence and phase between (a) ScandH17 and ScandT14, and (b) – (h) CMIP5/PMIP3 simulations of temperature and rainfall. The arrows indicate the relative phase relationship between two series; right (left) pointing arrow indicates in-phase (180 degrees out of phase) relationship. Significant coherence at 95% significance level is shown as thick contour.